Geosci. Model Dev., 19, 5155–5172, 2026
https://doi.org/10.5194/gmd-19-5155-2026

Geoscientific Model Development
Open Access
EGU

SIM-HOM (version 1.0): a mechanistic module for the formation of highly oxygenated organic molecules from isoprene, monoterpene and sesquiterpene evaluated with ADCHAM (version 1.0)

Liwen Yang[1], Wei Nie[1,2], Mikael Ehn[3], Chao Yan[2,4], Lubna Dada[5], Yuliang Liu[1,2], Pontus Roldin[6], and Aijun Ding[1,2,4]

[1]Joint International Research Laboratory of Atmospheric and Earth System Sciences,
School of Atmospheric Sciences, Nanjing University, Nanjing 210023, China
[2]National Observation and Research Station for Atmospheric Processes and Environmental Change in Yangtze River Delta,
Nanjing 210023, China
[3]Institute for Atmospheric and Earth System Research/Physics, Faculty of Science,
University of Helsinki, 00014 Helsinki, Finland
[4]Nanjing-Helsinki Institute in Atmospheric and Earth System Sciences, Nanjing University, Nanjing 210023, China
[5]Laboratory of Atmospheric Chemistry, Paul Scherrer Institute, 5232 Villigen, Switzerland
[6]Division of Combustion Physics, Department of Physics, Lund University, P.O. Box 118, 221 00 Lund, Sweden

Correspondence: Wei Nie (niewei@nju.edu.cn)

Received: 6 August 2025 – Discussion started: 18 November 2025
Revised: 16 March 2026 – Accepted: 10 April 2026 – Published: 16 June 2026

Abstract. Biogenic volatile organic compounds (BVOCs), including isoprene, monoterpenes, and sesquiterpenes, are emitted in large quantities and play a critical role in atmospheric chemistry. They contribute to the formation of highly oxygenated organic molecules (HOM), which are essential for new particle formation (NPF) and secondary organic aerosol (SOA) formation. However, current models often oversimplify the oxidation pathways of these compounds, leading to inaccuracies in predicting HOM composition and concentrations. To address this gap, we developed a mechanistic module, SIM-HOM (Sesquiterpene, Isoprene and Monoterpene-derived HOM mechanism), based on Master Chemical Mechanism (MCM), that explicitly incorporates autoxidation processes, detailed fragmentation pathways, and RO_2–RO_2 interactions for isoprene, monoterpene, and sesquiterpenes. The updated module was validated using experimental data from the Cosmics Leaving OUtdoor Droplets (CLOUD) chamber, demonstrating substantial improvements in simulating HOM concentrations under various conditions. Specifically, it significantly improves the simulation of highly oxidized isoprene products, resolves discrepancies in monoterpene-derived HOM distributions, and provides the first comprehensive parameterization of sesquiterpene oxidation products. The model also captures the HOM formation under mixed precursor conditions. These advancements underscore the importance of incorporating detailed molecular-level reaction mechanisms into atmospheric models. Future work should focus on refining branching ratios for critical reactions and investigating the influence of temperature and nitrogen oxides on HOM formation, and expanding the mechanism to include additional BVOC classes. Our findings provide a robust foundation for improving global atmospheric simulations of SOA formation and climate interactions.

1 Introduction

The continental boundary layer is profoundly influenced by biogenic volatile organic compounds (BVOC) emitted by vegetation. BVOC encompass diverse compounds, including isoprene, terpenes, and related species, with specific types varying by vegetation type and environmental conditions. The global annual emission flux of isoprene (C_5H_8) reaches up to 594 Tg, while monoterpenes ($C_{10}H_{16}$) are emitted approximately 95 Tg annually, sustaining mixing ratio

from parts per billion (ppb) levels ppb to hundreds of parts per trillion (ppt). Collectively, isoprene and monoterpenes contribute about 80 % of total BVOC emissions (Sindelarova et al., 2014). Sesquiterpenes, such as β-caryophyllene, are emitted around 20 Tg annually and are highly reactive compounds with a C_{15} skeleton. These BVOCs react rapidly with atmospheric oxidants, including hydroxyl radicals (OH), ozone (O_3), and nitrate radicals (NO_3), producing low-volatility oxygenated vapors. Among these, highly oxygenated organic molecules (HOM), are particular important as they significantly contribute to particle nucleation (Kirkby et al., 2016; Riccobono et al., 2014; Lehtipalo et al., 2018; Liu et al., 2024), growth (Simon et al., 2020; Stolzenburg et al., 2018; Trostl et al., 2016), and secondary organic aerosol (SOA) formation (Ehn et al., 2014; Nie et al., 2022; Liu et al., 2023; Sun et al., 2025).

Peroxy radicals (RO_2) are critical intermediates in the atmospheric oxidation of BVOC and play a central role in the formation of HOM. Under typical atmospheric conditions, a subset of RO_2 are produced by the oxidation of monoterpenes and sesquiterpenes by O_3 or OH can undergo rapid autoxidation during which internal H-shift and subsequent O_2 additions lead to the formation of multifunctional, low-volatility compounds (Iyer et al., 2021; Berndt et al., 2016; Shen et al., 2022; Richters et al., 2016b). The autoxidation rate is strongly sensitive to molecular structure, varying by several orders of magnitude depending on functional groups, and shows significant positive temperature dependence (Crounse et al., 2013; Praske et al., 2018; Moller et al., 2016; Jorgensen et al., 2016; Knap and Jorgensen, 2017; Otkjaer et al., 2018). Concurrently, autoxidation competes with bimolecular reactions involving NO_x, HO_2, and other RO_2 (Yang et al., 2025b). The RO_2–HO_2 reaction typically leads to the formation of hydroperoxides, which can contribute to HOM formation or undergo further reaction. Additionally, RO_2–RO_2 can result in the formation of HOM monomers, where two RO_2 react to produce two new molecules, often with one less oxygen atom than their precursors. RO_2–RO_2 reactions can also form HOM dimers (Heinritzi et al., 2020; Berndt et al., 2018; Ng et al., 2008), which are less volatile than HOM monomers and play a pivotal role in NPF and SOA formation. The influence of nitrogen oxides (NO_x) on HOM formation is complex: NO exhibits a nonlinear effect for cyclic monoterpenes, promoting HOM formation at low concentrations but inhibiting it at higher levels (Nie et al., 2023); whereas for isoprene, HOM formation may increase with NO (Berndt et al., 2025). NO_2 tends to suppress HOM formation by consuming acyl RO_2. Therefore, an accurate depiction of HOM formation requires consideration of autoxidation reactions and its competition with bimolecular RO_2 reactions, which are influenced by atmospheric composition, temperature, and the structure of the oxidizing molecules. Studies on the HOM formation from isoprene are limited because of its smaller molecular weight (Shen et al., 2024; Zhao et al., 2021; Wang et al., 2018; Xu et al., 2021; Curtius et al., 2024; Nie et al., 2022; Liu et al., 2021). It can suppress HOM formation by scavenging large RO_2 radicals formed from the oxidation of other VOCs (Heinritzi et al., 2020; McFiggans et al., 2019).

Insights into HOM formation mechanisms have highlighted the need to quantify their roles under varying atmospheric conditions. This has made possible by recent experimental advances, which have driven the development of numerical models primarily targeting HOM mechanisms from monoterpenes. Computationally efficient model like the radical two-dimensional Volatility Basic Set (radical-VBS) by Schervish and Donahue (2020), Schervish et al. (2024) and CRI-HOM (Weber et al., 2020) have been implemented in some large-scale models. These frameworks are designed to represent the overall formation and partitioning behavior of HOM using parameterized volatility distributions and oxidation pathways, rather than explicitly tracking individual molecules. While grounded in mechanistic understanding, their simplified representation may omit potential important aspects of chemical complexity, such as the role of specific RO_2 reaction pathways or the molecular identity of condensing vapors. Conversely, quasi-explicit approaches, such as the method by Roldin et al. (2019), provide detailed autoxidation chemistry but lack comprehensive descriptions of fragmentation products. For isoprene oxidation mechanisms, comprehensive models like the Master Chemical Mechanism (MCM) (Jenkin et al., 2015) and Caltech isoprene mechanisms (Wennberg et al., 2018) incorporate detailed representations of isoprene chemistry, consisting of hundreds of species (up to 602 in MCMv3.3.1 and 404 in the Caltech mechanism) and approximately 1000 reactions. While these existing models emphasize radical budget, carbon cycling and SOA contributions, they often do not resolve the specific HOM formation or accretion products in detail, due to their limited parameterizations. Sesquiterpenes, though often omitted from current models, can exhibit HOM yields of around 2 % (Richters et al., 2016a; Jokinen et al., 2016) under laboratory conditions. Given their 15-carbon structure, the resulting oxidation products are lower volatile than those from smaller VOCs, allowing even modest HOM yields to contribute efficiently to particle-phase mass and new particle growth.

Building upon these foundational studies, this study develops a unified and mechanistically detailed mechanism, SIM-HOM (Sesquiterpene, Isoprene, and Monoterpene-derived HOM mechanism) that extends HOM modeling to include not only monoterpenes and isoprene, but also sesquiterpenes, an often overlooked yet potentially important contributor due to their low volatility oxidation products (Dada et al., 2023). The model incorporates autoxidation and interactions among RO_2 radicals from various VOCs, enabling a more comprehensive representation of HOM formation under atmospherically relevant conditions. Section 2 details the model development based on existing gas-phase chemical mechanisms and theoretical studies. Section 3 discusses the model valida-

tion using the experiment data from Cosmics Leaving Outdoor Droplets (CLOUD) chamber, and section 4 summarizes this study and provides recommendations for future research.

2 Mechanism development

The mechanism developed in this study is primarily based on the MCM framework, chosen for its comprehensive representation of organic compounds degradation in the troposphere and its ability to incorporate a wide range of atmospheric chemical reactions with detailed kinetic and mechanistic data. Within its framework, the gas-phase chemistry of isoprene was refined using updates from the Caltech isoprene mechanism, focusing on the autoxidation pathway and HOM formation. Monoterpene oxidation was addressed using modifications from the Peroxy Radical Autoxidation Mechanism (PRAM), emphasizing fragmentations and ester formation as an accretion product. For sesquiterpenes, a dedicated module was developed, leveraging both theoretical and experimental data to represent its distinctive chemical pathways to HOM formation. Additionally, we incorporated detailed interactions between different RO_2 species, including dimer formation. Figure 1 illustrates the primary framework of this mechanism, with specific attention to the roles of unimolecular and bimolecular reactions in driving HOM production. Detailed modifications to the base mechanism are described in the following sections.

2.1 Extension of isoprene oxidation mechanism

In recent decades, significant advancements have been made in understanding the oxidation mechanisms of isoprene, due to its key role in atmospheric chemistry and its extremely high abundance in the atmosphere. As the most emitted BVOC globally, isoprene has been widely recognized as a significant SOA precursor, forming specific intermediates such as isoprene-epoxydiol (IEPOX) (Paulot et al., 2009; Nguyen et al., 2014) and methacryloyl peroxynitrate (MPAN) (Nguyen et al., 2015), in addition to highly functionalized low-volatility compounds (Krechmer et al., 2015; D'Arnbro et al., 2017; Xu et al., 2021).

Accurately representing the isoprene chemistry in large-scale atmospheric models is crucial but remains challenging due to the complex reaction mechanisms. MCM, through continuous updates, provides an almost complete compilation of isoprene's degradation pathways. Additionally, Wennberg et al. (2018) conducted a systematic review of current knowledge on isoprene chemistry, resulting in the development of the Caltech isoprene mechanism – a detailed reaction framework capable of dynamically simulating the allylic and peroxy radical systems formed when isoprene reacts with OH radicals (Wennberg et al., 2018). Compared to earlier mechanisms, the Caltech isoprene mechanism introduces significant advancements, including the incorporation of reversible O_2 addition to allyl radicals, the identification of new products from 1,6–H shifts in *Z*–*δ*–OH–peroxy radicals, and a reduced yield of C_5-hydroperoxy-aldehydes (HPALD). Furthermore, it includes more intramolecular H-shift processes, such as rapid peroxyl-hydroperoxyl (RO_2–OOH) shifts, which enhance OH recycling rates under low-nitrogen conditions. Despite these advancements, MCM provides a more detailed treatment of isoprene chemistry, including more comprehensive RO_2–RO_2 reactions and improved photolysis processes. The photolysis rate constants in MCM are calculated by integrating light flux over specific wavelengths, enabling accurate representation of photolysis under varying atmospheric conditions. In contrast, the Caltech mechanism calculates photolysis rates using a simplified coefficient, "sun", which relies on sunrise and sunset times. While effective for outdoor scenarios, this approach does not adequately capture the intricacies of controlled laboratory illumination, making MCM the preferred mechanism for laboratory-based simulations.

To exploit the strengths of both mechanisms, we integrated the MCM and Caltech isoprene mechanisms in our framework. This posed significant challenges due to differences in species naming conventions between the two frameworks. In the MCM, compounds are named systematically based on their chemical structure and assigned a unique identifier, whereas the Caltech mechanism employs a naming system based on the carbon skeleton and functional group positions. As a result, careful mapping of chemical species between the two mechanisms was required to bridge these discrepancies (see Supplement for details). This integrated approach allows us to harness the complementary advantages of both mechanisms for a more robust representation of isoprene chemistry.

Despite these improvements, the descriptions of HOM production from the oxidation of isoprene remain incomplete. To address this gap, we incorporated autoxidation pathways for specific high-yield RO_2 formed during isoprene oxidation, which are crucial intermediates in isoprene oxidation. The key RO_2 radicals considered include those substituted with =O, −OH, and −OOH groups, which originate from isoprene hydroxyperoxyl radicals (ISOPOO) and RO_2 species formed following a 1,6 α-hydroxy H-shift in two *Z*–*δ*–ISOPOO isomers. The rapid H-shift reactions of these high-yield RO_2 radicals are critical, as they allow for the production of stable, low-volatility products under typical atmospheric conditions, making them particularly potent for HOM formation.

For these H-shift reactions to compete effectively with bimolecular reactions involving NO, HO_2, and other RO_2, unimolecular reaction rate constants need to reach approximately $\sim 10^{-2}\ s^{-1}$ or higher. Reported H-shift rates for these radicals cover a wide range, from 8.2×10^{-2} to $3.0 \times 10^{5}\ s^{-1}$ at 298 K (Moller et al., 2019), with hydroperoxides exhibiting notably faster rate. While the Caltech isoprene mechanism assumes alkyl radicals predominantly fragment into smaller products, thus limiting HOM formation, we intro-

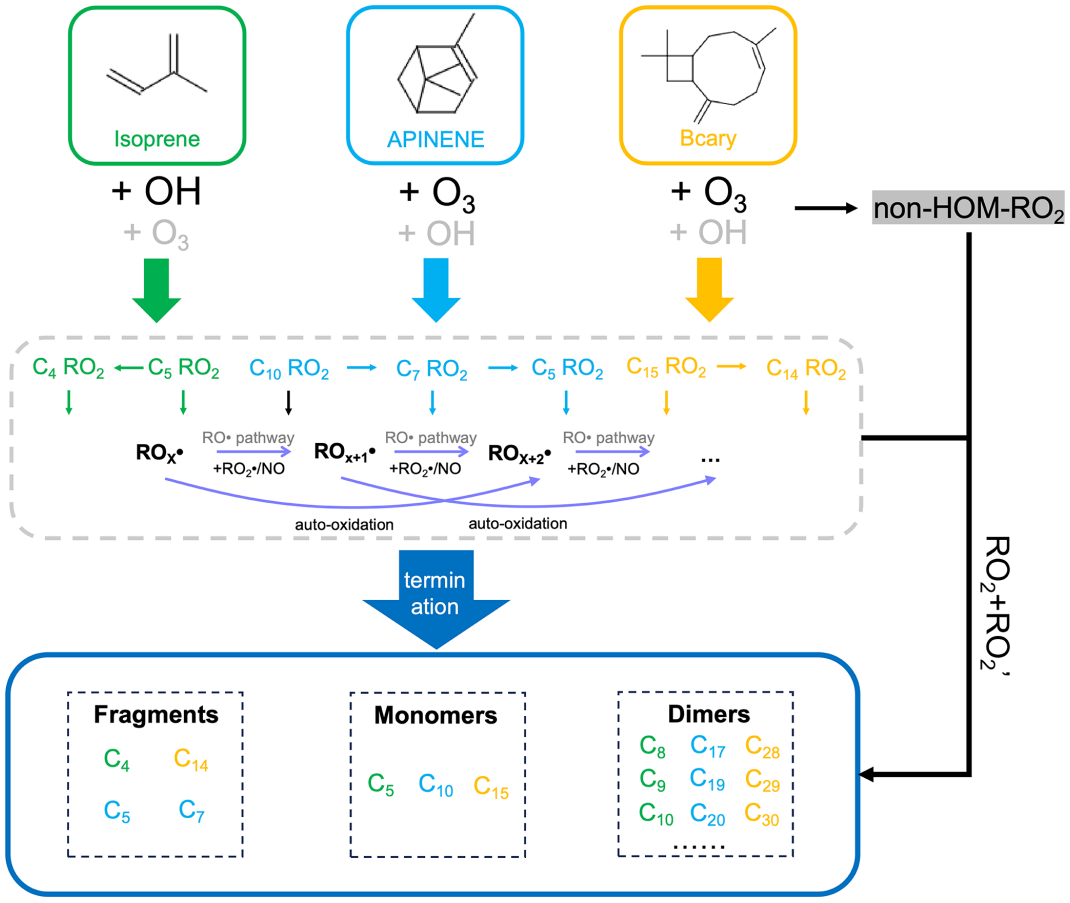

Figure 1. Schematic plot showing the mechanism of HOM formation via the oxidation of isoprene, monoterpenes and sesquiterpenes in the absence of NO_x. Isoprene is primarily oxidized by OH, while monoterpenes and sesquiterpenes are primarily oxidized by O_3. A small fraction of RO_2 can undergo autoxidation (defined as p-HOM-RO_2, colored font in the figure), and the other fraction of RO_2 that cannot undergo autoxidation (defined as non-HOM-RO_2, grey-bottomed font in the figure). p-HOM-RO_2 can undergo both unimolecular and bimolecular reactions, and both can form alkoxyl radicals, which can fragment or isomerize. For the dimer formation, we only consider them from RO_2–RO_2 reactions between p-HOM-RO_2 and non-HOM-RO_2.

duced an oxygen addition pathway to alkyl radicals, as suggested in Wang et al. (2018). This modification introduces a competing reaction pathway that can produce new RO_2 species, counterbalancing the dominance of fragmentation. Subsequent bimolecular reactions involving these RO_2 species were implemented based on the work of Jenkin et al. (2019).

Although OH oxidation overwhelmingly dominates the removal of isoprene from the atmosphere, O_3 oxidation accounts for approximately 10 % of isoprene's global loss (Bates and Jacob, 2019). Previous models primarily focused on its contributions to the formation of methyl vinyl ketone (MVK), methacrolein (MACR), CH_2OO (C_1 SCI), and OH, while largely neglecting its potential contribution to HOM formation. Here, we adopted a simplified approach similar to that of Schervish et al. (2024), assuming that only a small fraction of RO_2 radicals are capable of undergoing autoxidation. These RO_2 radicals can subsequently participate in unimolecular or bimolecular reactions, with some contributing to the HOM formation.

2.2 Improvement of monoterpene oxidation mechanism

Our model extends the first comprehensive Peroxy Radical Autoxidation Mechanism (PRAM) developed by Roldin et al. (2019). PRAM meticulously simulates the autoxidation processes of RO_2 formed from monoterpene oxidation. This mechanism has demonstrated strong agreement with observed HOM concentrations, SOA mass concentrations, and NPF in boreal forest simulations. However, the original PRAM only considered the HOM formation pathway via monoterpene oxidation by O_3 and OH. Nie et al. (2023)later expanded this mechanism by incorporating NO_3-initiated oxidation pathway to the original mechanism, which mainly includes the autoxidation of monoterpenes by NO_3 to form RO_2; the reaction of RO_2 with NO_3 to form RO radicals

(though this pathway is negligible under most environmental conditions) and bimolecular termination reactions between NO_2 and specific RO_2 (e.g., acyl RO_2) (Nie et al., 2023).

In this study, we further optimize the key oxidation pathways of monoterpenes, with a particular focus on α-pinene ozonolysis, which serves as a representative case due to its atmospheric relevance and detailed mechanistic understanding. Conventional mechanisms propose that α-pinene ozonolysis begins with the decomposition of the primary ozonide into a carbonyl-substituted Criegee Intermediate (CI). Three isomeric forms of this CI can undergo a 1,4 H-shift to produce vinyl hydroperoxide (VHP). The VHP subsequently decomposes into a vinoxy radical, which reacts with O_2 to form a RO_2 radical. However, under typical conditions, the isomerization of this RO_2 radical is too slow to explain the observed rapid formation of HOMs. To address this, Iyer et al. (2021) proposed a critical solution by introducing a chemically activated ring-opening reaction of one of the vinoxy radicals. This reaction leads to the rapid formation of an endoperoxide and a RO_2 radical with a high oxygen content (containing 8 oxygen atoms). The PRAM mechanism incorporates this modification and further details the progressive increase in oxygen atoms within the molecule through consecutive intramolecular RO_2 H-shifts and O_2 additions during autoxidation. This autoxidation chain ultimately terminates through bimolecular reactions with NO, HO_2, or other RO_2 radicals, forming a variety of products such as alkoxy radicals, closed-shell HOM monomers, or dimers. Once alkoxy radicals are formed, they may undergo further transformations. For example, they can isomerize into hydroxy-substituted alkyl radicals, which subsequently react with O_2 to form new RO_2 species, or they may form closed-shell HOM monomers with additional carbonyl groups. Alternatively, they may decompose into more volatile species. A specific example of these fragment products includes the MCM-modeled RO_2 species $C717O_2$ (an RO_2), and smaller volatile species like acetone (CH_3COCH_3).

In our improved model, we incorporated the C_7-fragment due to recent studies indicate that early-formed addition products retain sufficient energy to overcome transition state barriers, leading to the formation of a significant amount of alkyl radicals with an endoperoxide group (EPO). Unlike the traditional view that excess energy dissipates in the next O_2 addition step, Yang et al. (2025a) demonstrated that EPO formation enables rearrangement pathways involving alkoxy radicals with epoxide groups (AOE). Their study identified that cleavage reactions from these intermediates, which yield acetone and C_7 products (AE-C_7), are the fastest. Furthermore, the O_2 addition products (RO_2) formed from AE-C_7 and AE-C_{10} contain multiple active sites for H-shift, facilitating further autoxidation. These findings provide key insights into the competition between unimolecular H-shift reactions and bimolecular sinks, such as reactions with NO and HO_2. Additionally, the contribution of AE-C_7 and AE-C_{10} derivatives explains observed peaks in mass spectrometry corresponding to C_7-HOMs.

We also incorporated RO_2–Kb β-cleavage and CH_2O loss to better represent the formation of C_{19} accretion products, like $C_{19}H_{28}O_x$ and $C_{19}H_{30}O_x$, as observed in experiments by Berndt et al. (2018). These products are formed through RO_2 self- and cross-reactions involving CH_2O loss. Furthermore, experiments that isolated OH oxidation revealed that these C_{19} accretion products are not formed through pure OH-mediated processes, but rather arise specifically from O_3-derived RO_2 radicals (Peräkylä et al., 2023; Kenseth et al., 2023). Our updated model explicitly accounts for these distinctions, differentiating the contributions of OH- versus O_3-derived RO_2 radicals in the formation of HOM accretion products.

2.3 Development of sesquiterpene oxidation mechanism

Prior to our work, HOM formation from sesquiterpenes lacked a dedicated module in atmospheric models. To address this, we developed a comprehensive framework based on the reaction pathways proposed by Richters et al. (2016b), integrating key processes derived from existing knowledge to better represent the oxidation chemistry of sesquiterpenes. Given that β-caryophyllene is the only sesquiterpene included in MCM, our development focuses exclusively on this compound.

The ozonolysis of β-caryophyllene begins with an exothermic reaction between O_3 and the double bonds of sesquiterpene molecules, forming CIs with significant excess energy. These chemically activated CIs can either stabilize through collisions with other molecules or undergo unimolecular reactions. Stable CIs may also engage in bimolecular reactions, initiating a variety of pathways that eventually lead to HOM formation. A critical step involves the isomerization of CIs into vinyl hydroperoxide, which further decomposes by releasing OH radicals, producing alkyl radicals as intermediates. The alkyl radicals rapidly react with O_2, forming the first generation of RO_2 radical.

The fate of these initial RO_2 radicals branch into several pathways. In one major pathway, the RO_2 radical undergoes intramolecular H-shifts followed by O_2 addition, resulting in new RO_2 radicals that resemble the first-generation p-HOM-RO_2 species observed in monoterpene ozonolysis. These products typically include hydroperoxide ($-$OOH) functionalities. Alternatively, RO_2 radicals can attack the remaining double bond in the sesquiterpene structure. This process leads to the formation of endoperoxides and additional alkyl radicals, which subsequently react with O_2 to form new RO_2 radicals, though these lack the -OOH functional group. Further reaction pathways are also possible. For instance, RO_2 radicals may undergo additional intramolecular H-shifts, resulting in the formation of closed-shell products along with the release of OH radicals; or the subsequent O_2 addition

after H-shift forms a new RO_2. Another pathway involves internal RO_2 reactions with the remaining double bond, which can generate cyclic R radicals. These cyclic radicals then react with O_2, producing the next generation of RO_2 radicals.

Epoxide formation is another potential pathway, where an epoxide ring forms within the molecule, followed by cleavage of the acyl alkoxy functionality and the expulsion of CO_2. This step yields alkyl radicals that rapidly react with O_2 to form new RO_2 species. These RO_2 radicals can then enter further autoxidation processes, involving a series of intramolecular hydrogen transfer reactions and successive O_2 additions, to produce higher-generation RO_2 species.

By systematically integrating these reaction pathways into our model, we developed a robust framework to simulate HOM formation from sesquiterpene ozonolysis. The inclusion of detailed autoxidation chemistry, along with pathways involving both -OOH and non-OOH functional group formation, ensures a more comprehensive representation of the sesquiterpene oxidation process and its contribution to atmospheric HOM and SOA formation.

2.4 RO_2 cross reactions in mixed VOC system

In real atmospheric conditions, VOC mixtures produce a variety of RO_2 radicals that can react with each other to form RO, closed-shell monomers, or dimers. Given the vast number of RO_2 species in detailed chemical mechanisms, explicitly representing all possible cross-reactions is impractical. To address this, MCM uses a simplified approach, which assumes that all RO_2 radicals interact uniformly within a "RO_2 pool" at a collective rate. This is implemented using the parameter $\Sigma[RO_2]$, which represents the summed concentration of all RO_2 species. Within this framework, the total rate of all possible cross-reactions for a particular RO_2 radical is approximated as a pseudo-unimolecular reaction with a rate coefficient of $k \times \Sigma[RO_2]$. While this simplification reduces computational complexity, it overlooks the specific contributions of individual RO_2 combinations, particularly in processes like dimer formation. The CRI-HOM model addresses dimerization by treating it as a simplified reaction in which one RO_2 radical produces half of the total dimer product. Although efficient, this approach fails to account for differences in how specific RO_2 combinations influence product distributions.

In our improved model, we redefine dimerization as a specific bimolecular reaction between distinct RO_2 species. To reduce complexity, we focus on the interactions between two key types of RO_2: those capable of autoxidation and those that cannot undergo autoxidation (as represented in MCM). Autoxidizable RO_2 radicals, due to their higher degree of functionalization, exhibit faster dimerization rates Berndt et al., 2018). Non-autoxidizable RO_2 radicals, which are generally present at higher concentrations, can serve as reaction partners in these bimolecular reactions. Reactions between two autoxidizable RO_2 are not explicitly represented, due to their extremely low concentrations, which makes their contribution to dimer formation negligible. Likewise, reactions between two non-autoxidizable RO_2 are not treated as explicit accretion product formation pathways due to due to their products are probably not HOM. Instead, these reactions remain represented within the generic RO_2 loss framework of the RO_2 pool, where they contribute to closed-shell monomer formation through the pseudo-unimolecular reaction scheme. In this way, the total RO_2–RO_2 reaction flux among all RO_2 species is still accounted for, while only those combinations most relevant for HOM dimer formation are treated explicitly.

$RO_2 + RO_2$ rate coefficients are assigned according to the overall oxidation state and molecular size of the RO_2 radicals, using the number of oxygen atoms as a proxy for the degree of functionalization. This approach is consistent with the parameterization described above, where more highly oxygenated and generally larger RO_2 radicals are assumed to exhibit higher reactivity in $RO_2 + RO_2$ reactions. SIM-HOM uses $RO_2 + RO_2$ reaction rates leading to closed-shell monomer products in the range of 1×10^{-12} to 1.5×10^{-11} $cm^3\ s^{-1}$ and $RO_2 + RO_2$ reactions leading to HOM dimers in the range of 1×10^{-14} to 1.5×10^{-12} $cm^3\ s^{-1}$. This choice reflects the generally smaller branching fraction of the accretion channel relative to the formation of monomer products. As a result, the effective branching ratio toward accretion products in the model is typically on the order of $\sim 10\,\%$, consistent with recent experimental and theoretical studies (Murphy et al., 2025; Berndt et al., 2018). Because these dimers arise from explicit bimolecular reactions, the identities of these products are determined by the specific pair of reacting RO_2 precursors. This approach balances computational efficiency with improved accuracy, capturing the variability in RO_2 reactions and their impact on product distributions, particularly in mixed VOC systems.

2.5 Summary of the model improvements

We implemented several key updates to the model, focusing on the autoxidation pathway, RO_2–RO_2 interaction, fragmentation and termination processes. Together, these enhancements provide a more accurate and comprehensive representation of atmospheric oxidation, enabling better simulation of VOC oxidation and HOM formation:

1. Expanded Autoxidation Pathways: we refined the autoxidation scheme for isoprene, monoterpenes, and sesquiterpenes by incorporating recent experimental and theoretical advancements. Key updates include (1) High-yield RO_2 autoxidation reactions for isoprene oxidation; (2) Extended formation and autoxidation pathways for C_7-RO_2 species in monoterpene oxidation; (3) Integration of new autoxidation and HOM formation processes for sesquiterpenes, building on the MCM framework.

2. Improved RO_2–RO_2 Interactions: for permutation reactions, we maintained MCM's computationally efficient method. However, for dimer formation, we moved beyond the simplified treatments used in mechanisms like CRI-HOM. Our model explicitly parameterizes RO_2–RO_2 interactions based on their VOC origins and incorporates β-cleavage reactions for RO_2 from monoterpene ozonolysis during dimerization. This provides a more detailed representation of dimer distributions and the behavior of mixed VOC systems.

3. Updated Fragmentation and Termination Pathways: we incorporated detailed fragmentation mechanisms for monoterpene and sesquiterpene oxidation products, enabling more accurate predictions of experimental product distributions. Additionally, new pathways for alkoxy radical formation and subsequent secondary RO_2 radicals were introduced, improving the representation of carbon distribution among the oxidized products.

3 Model validation based on CLOUD experiments

We validated the constructed model using experimental data from the Cosmic Leave Outdoor Droplet Chamber (CLOUD) at CERN. The experiments were conducted in a 26.1 cm^3 stainless steel chamber that can simulate diverse atmospheric conditions under well-controlled environments. Specifically, we utilized data from the CLOUD 11 campaign conducted in the fall of 2016 (Dada et al., 2023; Heinritzi et al., 2020). These experiments included oxidation of single precursors (pure isoprene, α-pinene, and β-caryophyllene) and their mixtures, such as α-pinene and isoprene, or α-pinene, isoprene, and β-caryophyllene. Table 1 summarizes the experimental conditions. For the mixed experiments, the precursor molar ratio (sesquiterpene: monoterpene: isoprene) was set to 1 : 6 : 50 to mimic typical BVOC emissions in the atmosphere. Most pure α-pinene and β-caryophyllene experiments were performed under dark conditions, with OH concentration of approximately 1×10^6 cm^{-3}, formed primarily via the BVOCs reactions with O_3. When isoprene was added, OH is predominantly consumed by isoprene, resulting in a further lower OH concentration. To increase OH concentrations, Hamamatsu UV lamps (UVH) and UV excimer lasers (UVX) were employed. No NO_x was introduced in the experiments, effectively excluding NO_3 oxidation pathways. The CLOUD chamber is one of the most advanced reactors for replicating atmospheric conditions, ensuring that the lifetime and reaction pathways of p-HOM-RO_2 in the chamber closely resemble those in the real atmosphere. This allows p-HOM-RO_2 to undergo sufficient autoxidation. The oxidation products, i.e., oxygenated organic molecules, were measured using a nitrate chemical ionization atmospheric pressure interface time-of-flight (CI-API-ToF) mass spectrometer.

Our initial chemical mechanism did not account for deposition or condensation onto pre-existing aerosol surfaces. To address this limitation and isolate the effects of gas-phase chemistry, we coupled the chemical mechanism with the Aerosol Dynamics, gas- and particle-phase chemistry model for laboratory CHAMber studies (ADCHAM) (Roldin et al., 2014). ADCHAM integrates modules for aerosol dynamics, particle-phase chemistry, and a kinetic multilayer model to account for diffusion-limited transport between the gas phase, particle surface, and particle bulk. Once the chamber reactions reached steady-state, we simulated the HOM concentrations and compared the results with experimental data. By iteratively adjusting the rate constants for autoxidation and accretion product formation, we refined the chemical mechanism to achieve the best agreement with experimental observations.

3.1 Overall comparison

To assess the model's performance under varying environmental conditions, we calculated the relative error of HOM concentrations by normalizing the difference between observed and simulated concentrations. Only species with concentrations exceeding 5×10^4 cm^{-3} (the CI-APi-ToF detection limit) were considered. As shown in Fig. 2a, the relative errors (defined as the difference between modeled and measured HOM concentrations normalized by the measurements) are illustrated as box plots. They remain close to 0 under most conditions, indicating strong agreement between model and measurements. However, in the mixed system of three VOCs (IP + MT + SQT), particularly at low VOC concentrations, larger discrepancies appear. This may be attributed to photolysis of oxidation products by UVH lamps, which is not explicitly considered in detail, leading to deviations in HOM predictions. The number of selected data points (gray dashed line) also varies across different conditions, influencing error estimates.

Figure 2b compares the simulated and observed HOM concentrations across different VOC systems. The total HOM concentration varies significantly across different precursors. The isoprene system produces relatively lower HOM concentrations compared to monoterpene and sesquiterpene systems, consistent with the expected differences in oxidation pathways and HOM formation efficiency. The monoterpene system exhibits the highest HOM concentrations, particularly at higher precursor concentrations, followed by the sesquiterpene system. In mixed systems, including the isoprene-monoterpene system (Mix I) and the three-VOC mixture (Mix II), the total HOM concentration increases compared to the isoprene-only system, reflecting the contribution of monoterpenes and sesquiterpenes. The model successfully reproduces the general trends, capturing the HOM concentrations in isoprene, monoterpene, and sesquiterpene systems, as well as in mixed systems. However, overestimation is observed in some cases, particularly in low VOC concentration scenarios, as discussed earlier, likely due to incomplete representation of photolysis processes. Despite

Table 1. Summary of the experimental conditions used in this study. All experiments are performed at 5 °C and 40 % RH.

	Exp	Isoprene (ppt)	α-pinene (ppt)	Bcary (ppt)	O_3 (ppb)	UVH	UVX
Isoprene system	IP-4500	4456	0	0	37.5	off	off
	IP-4500	4214	0	0	41.5	off	on
Monoterpene system	MT-300	0	340	0	40.7	off	off
	MT-600	0	666	0	40.2	off	off
	MT-1200	0	1165	0	39.3	off	off
	MT-1200	0	1059	0	39.7	off	on
Sesquiterpene system	SQT-1.8	0	0	1.8	47.8	off	off
	SQT-3.3	0	0	3.3	48.5	off	off
	SQT-6.6	0	0	6.6	47.6	off	off
	SQT-6.6	0	0	6.6	48.7	on	off
Mixed system I: isoprene and monoterpene	Mix I-MT300	3962	317	0	44.9	off	off
	Mix I-MT600	3780	618	0	46.4	off	off
	Mix I-MT1200	3588	1116	0	47.6	off	off
	Mix I-MT1200	3396	1096	0	47.9	on	on
Mixed system II: isoprene, monoterpene and sesquiterpene	Mix II-Low	1471	303	3	45.6	on	off
	Mix II-Medium	2695	578	7.1	45.7	on	off
	Mix II-High	5749	1168	15.8	44.3	on	off
	Mix II-High	4578	974	15.8	44.3	on	on

these minor deviations, the overall variations in HOM production across different VOC regimes are well reproduced.

3.2 Isoprene system

In the pure isoprene system, the isoprene was continuously injected to maintain a concentration between 4 and 5 ppb, while O_3 was approximately 40 ppb, under both dark and illuminated conditions. We compared the simulation results from our improved module, MCM, the Caltech isoprene mechanism (Caltech), and their combination (MCM + Caltech). All models showed strong performance in predicting OH concentration (Fig. 3c).

Across different experimental conditions, our model exhibits significant advantages in capturing the distribution of highly oxygenated oxidation products compared to other models. For OOMs containing 5 oxygen atoms, all four models predicted concentrations notably higher than the experimental measurements (Fig. 3a and b), likely due to the reduced sensitivity of the NO_3^- CI-APi-ToF mass spectrometer towards OOMs with five or fewer oxygen atoms (Riva et al., 2019). For OOMs with six or seven oxygen atoms, the MCM model significantly overestimated their concentrations, while the Caltech model underestimated them. In contrast, our model closely matched the measured data, indicating superior accuracy in simulating these oxidized species. More importantly, for OOMs containing eight or more oxygen atoms, our model was the only one capable of capturing their formation, underscoring its ability to accurately represent the complex pathways of HOM formation during isoprene oxidation.

Recent studies have demonstrated that isoprene-derived highly oxygenated organic molecules (IP-HOMs) play a key role in new particle formation (NPF) in the upper troposphere (Curtius et al., 2024; Shen et al., 2024; Zha et al., 2024). Our model effectively simulates the formation of HOMs, underscoring its relevance for investigating the mechanisms of NPF and subsequent particle growth. However, the observed HOM spectrum in our chamber experiments differs from that of the atmosphere due to weak OH recycling, a consequence of the absence of NO_x and the predominantly dark or low-light experimental conditions. Atmospheric OH• levels during daytime typically remain above $10^6\,cm^{-3}$, even in the presence of isoprene, sustaining secondary oxidation processes. As a result, atmospheric isoprene oxidation predominantly produces $C_5H_{12}O_x$, $C_5H_{11}NO_x$ and $C_5H_{10}N_2O_x$ via second-generation OH oxidation from ISOPOOH and isoprene hydroxy nitrate (Curtius et al., 2024; Shen et al., 2024; Zha et al., 2024; Xu et al., 2021). In contrast, our experimental spectrum is dominated by $C_5H_{8-10}O_x$ (Fig. S2), derived from the mono- and bimolecular reaction of RO_2 formed directly via isoprene oxidation. A comparison of $C_5H_{12}O_x$ concentrations with other C_5 compounds (Fig. S3) further confirms that second-generation oxidation plays a minimal role in our experiments. Despite these differences, our model integrates all relevant oxidation pathways, providing a more comprehensive representation of isoprene oxidation chemistry.

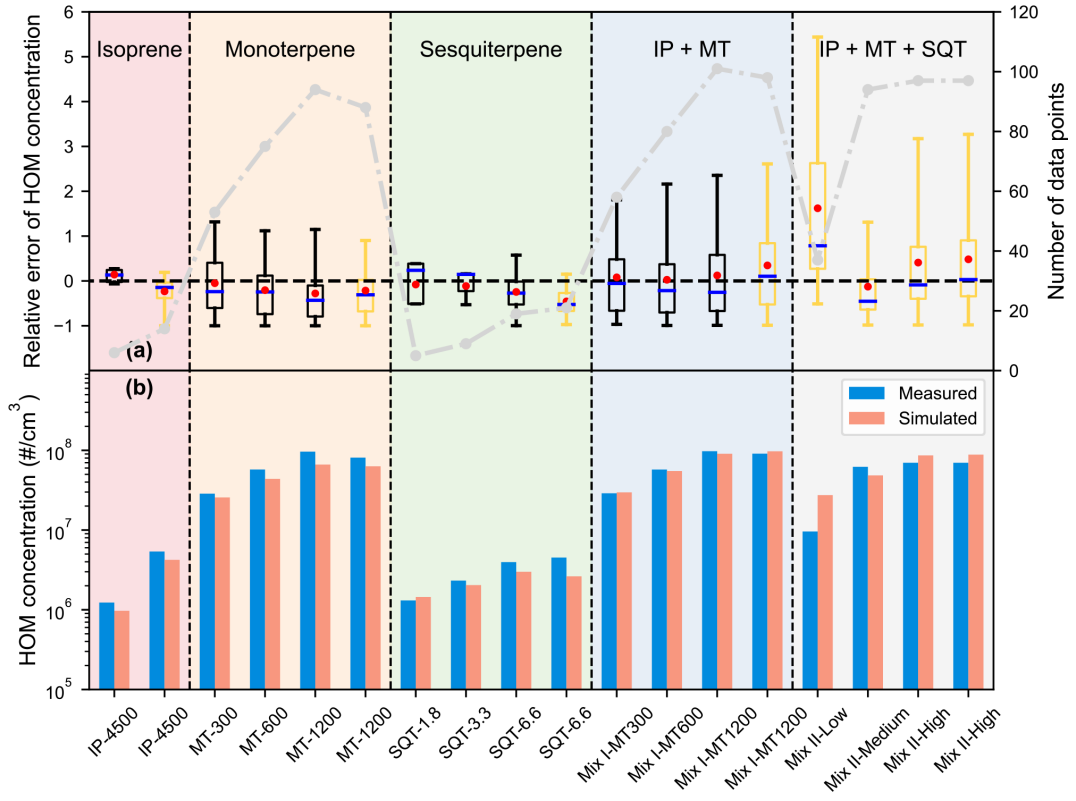

Figure 2. **(a)** Boxplots of relative errors and **(b)** comparison of simulated HOM and observations under different experimental conditions. From left to right, they represent pure isoprene, monoterpene, and sesquiterpene systems, the mixed system of isoprene, monoterpene, and the mixed system of the three VOCs. The specific experimental conditions are shown in Table 1. Boxplots represent medians, quartiles, and 5 %–95 % percentiles, with red circles indicating the median, where the boxes are black in dark conditions and yellow in light conditions. The grey line indicates the number of HOM with higher concentration than the detection limit under each experimental condition. Blue and outer circles indicate observed values, pink and inner circles indicate simulated values.

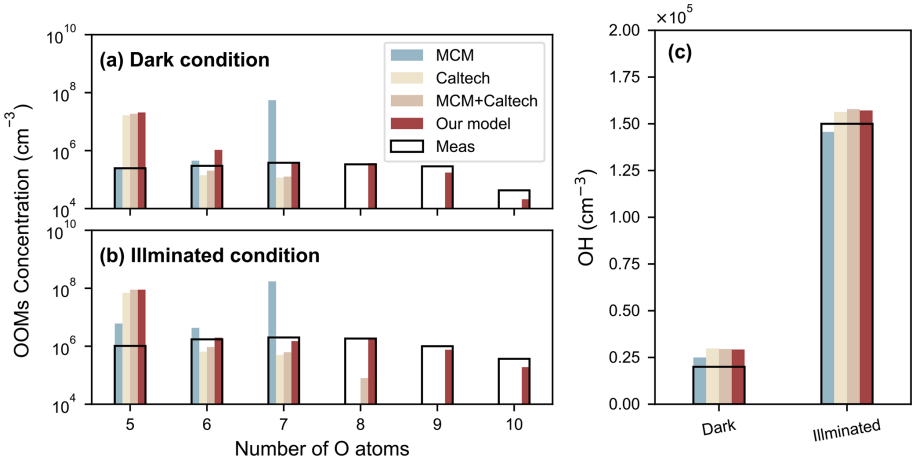

Figure 3. Comparison of measured and simulated results from four models (our improved model, MCM, Caltech, and MCM + Caltech): **(a)** oxidation products with varying numbers of oxygen atoms under dark conditions, **(b)** oxidation products under illuminated conditions, and **(c)** OH concentration under both dark and illuminated conditions.

3.3 Monoterpene system

Figure 4 presents the predicted oxidation products spectrum from our improved model alongside experimental measurement under different conditions. A detailed comparison with the experimental data demonstrates that our model achieves high accuracy in reproducing monoterpene oxidation processes. In particular, it effectively captures the formation of RO_2 radicals with 10 carbon atoms (C_{10}–RO_2) and accurately simulates their subsequent reaction pathways. Fragment simulation has traditionally been a challenge in numerical modeling. In our improved model, we incorporated C_7 fragments formation by incorporating recent findings on early-stage product cleavage (Yang et al., 2025a). The model successfully reproduces the isomerization of C_{10}–RO_2, leading to carbon skeleton cleavage and C_7-RO_2 formation, which undergoes autoxidation and termination to produce C_7–HOMs. Furthermore, C_7–RO_2 produces C_5–RO_2 through RO pathway, accurately simulating key fragment products such as $C_5H_6O_7$, validating the model's capability in capturing essential oxidation pathways.

Beyond accurately representing the main monomer and fragmentation product distributions, the model also exhibits significant improvements in simulating dimer formation. In particular, the enhanced formation of C_7–RO_2 has led to an improved prediction of $C_{17}H_{26}O_9$ concentration, which corresponds to the most abundant dimer observed in our measurements. Additionally, the incorporation of RO_2–Kb β-cleavage and CH_2O loss processes have contributed to the relatively high concentrations of $C_{19}H_{28}O_9$ and $C_{19}H_{28}O_{11}$ dimers. Despite these advancements, the model still slightly underestimates these dimer concentrations compared to experimental observations. Several factors may contribute to this discrepancy. First, the actual yield of RO_2–Kb is higher than estimated in MCM (Meder et al., 2025), leading to an underrepresentation of key dimer-forming precursors. Second, RO_2–Kb cleavage products may have a higher efficiency in forming accretion products compared to other RO_2, an aspect not fully accounted for in the current model. Third, additional RO_2 species beyond those currently considered may undergo similar cleavage reactions, contributing to dimer formation through pathways not yet incorporated (Peräkylä et al., 2023). Addressing these uncertainties by refining the branching ratios and reaction rate constants of dimerization pathways could help resolve these discrepancies and further improve the model's predictive capabilities.

3.4 Sesquiterpene system

Figure 5 shows that our newly developed sesquiterpene-HOM model is in strong agreement with the experimental data. During the validation process, we meticulously compared the model predictions with experimental results obtained under controlled conditions, ensuring that key chemical products – including fragmentation products, monomers, and dimers – were accurately represented. The model accurately captures the formation and transformation of these products, confirming its reliability in simulating sesquiterpene oxidation.

A key achievement of the model is its accurate prediction of $C_{15}H_{22}O_9$, the most abundant HOM molecule under these experimental conditions and a critical ELVOC contributing to NPF (Dada et al., 2023). This highlights the model's ability to capture the dominant oxidation pathways of sesquiterpenes. To comprehensively describe the reaction mechanism, we incorporated an epoxide formation step, in which CO_2 is expelled from the acyl alkoxy functional group of the intermediate, forming an alkyl radical that rapidly reacts with O_2 to form an RO_2 radical. This modification successfully explains the observed C_{14} fragmentation product, further improving the model's accuracy in reproducing experimental spectrum. However, while the model successfully reproduces the observed peaks for most monomers and fragments, it fails to predict $C_{10}H_{14}O_{10}$, which is detected at non-negligible concentrations in experiments. This discrepancy arises from the absence of reported formation pathways for this compound, suggesting that additional reaction mechanisms may need to be explored.

Regarding dimer formation, the model incorporates detailed RO_2 cross-reaction pathways. While the model provides a reasonable overall prediction, it overestimates the concentrations of lower-molecular-mass dimers while underestimating the most abundant dimers, such as $C_{29}H_{44}O_{12}$ and $C_{29}H_{46}O_{14}$. This suggests that refinements in the reaction rates governing dimerization processes-particular the relative contribution of RO_2–RO_2 from fragment RO_2 are necessary to achieve better agreement with observations. Additionally, the inclusion of alternative dimerization channels, such as those involving secondary oxidation, may be required to better represent the observed dimer distribution.

Overall, the strong agreement between model predictions and experimental data indicates that our model effectively captures the fundamental oxidation mechanism governing sesquiterpene-derived HOM formation. By incorporating detailed reaction pathways and refining key parameters, the model not only reproduces observed concentration but also provides mechanistic insights into HOM formation. These advancements establish our sesquiterpene-HOM module as a valuable tool for simulating complex chemistry under atmospheric conditions.

3.5 Mixed system

In this section, we compared the observed and simulated HOM concentrations in mixed systems under various conditions, including different VOC combinations, changes in VOC concentrations and the introduction of UV light (see Figs. S4 and S5). Across all cases, the simulations overall matched the observed HOM distributions, accurately reproducing key peaks and maintaining the expected carbon num-

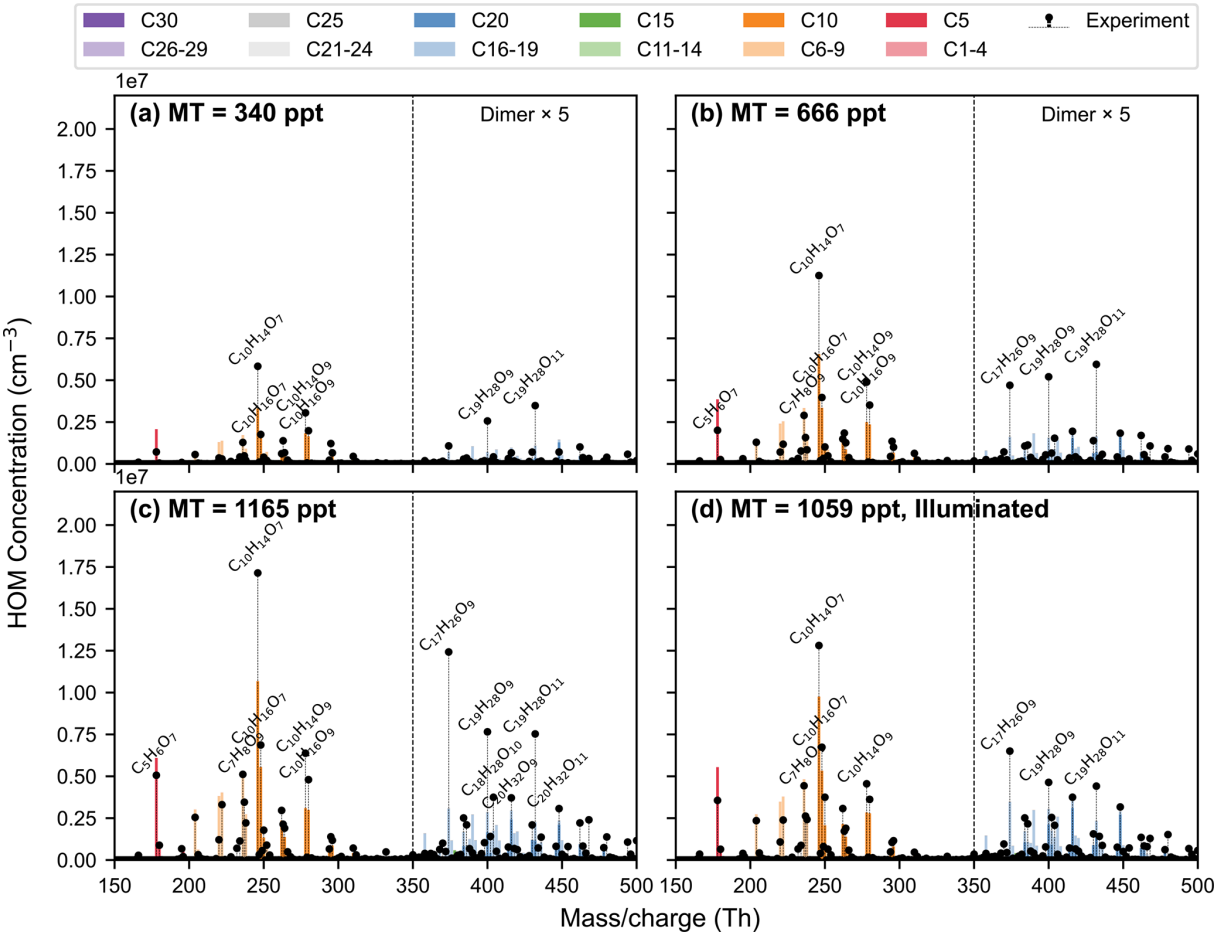

Figure 4. Comparisons between modeled and observed spectrum in α-pinene oxidation experiment with **(a)** 340 ppt, **(b)** 666 ppt, **(c)** 1165 ppt and **(d)** 1059 ppt α-pinene in **(a–c)** dark condition and **(d)** UV excimer laser (UVX) on. Mass/charge ratio is plotted in units of thomsons (Th) and it should be noted that the nitrate reagent ions has been removed from mass.

ber distributions. Additionally, we analyzed the variation in HOM concentrations with different carbon numbers for four representative mixing conditions: (1) a mixture of isoprene and monoterpenes (Mix I-MT600), (2) an increased monoterpene concentration (Mix I-MT1200), (3) the introduction of UV light (Mix I-MT1200, Illuminated), and (4) the subsequent addition of sesquiterpenes (Mix II-High, Illuminated).

In the initial isoprene–monoterpene mixture, oxidation led to a diverse range of HOMs from both C_5– and C_{10}–RO_2 pathways (Fig. S4a). Increasing the monoterpene concentration enhanced HOM formation, particularly for monoterpene-derived species, like $C_{6–10}$– and $C_{16–20}$–HOMs (from Mix I-MT600 to Mix I-MT1200, Fig. 6b and d). The introduction of UV light shifted the HOM distribution by promoting isoprene oxidation, leading to an increase in $C_{1–5}$- and $C_{1–15}$-HOMs (from Mix I-MT1200 to Mix I-MT1200, illuminated, Fig. 6a and c) while reducing monoterpene-derived termination products, in particular dimers with more than 15 carbon atoms. However, the model underestimated $C_{11–15}$–HOM concentrations, likely due to an underrepresentation of cross-reaction between isoprene-derived and monoterpene-derived RO_2. The addition of sesquiterpenes further altered HOM distribution, notably increasing $C_{11–15}$–HOM (Fig. 6c), suggesting sesquiterpenes exhibit a higher propensity for autoxidation and further amplifying these product channels. However, the significant decrease in $C_{16–30}$–HOM concentration observed in three-VOC mixture, which was not reflected in the simulations (Fig. 6d), could be attributed to the overestimated rate of dimer formation involving sesquiterpenes. This shift was likely driven by the competitive consumption of available RO_2 radicals, which are reflected in both observations and models. Our model's ability to simulate key features – such as the redistribution of HOM classes due to competitive RO_2 chemistry – demonstrates its robustness in simulating the oxidation of complex VOC mixtures. This agreement highlights the model's capability to provide mechanistic insights into HOM formation under varied atmospheric conditions.

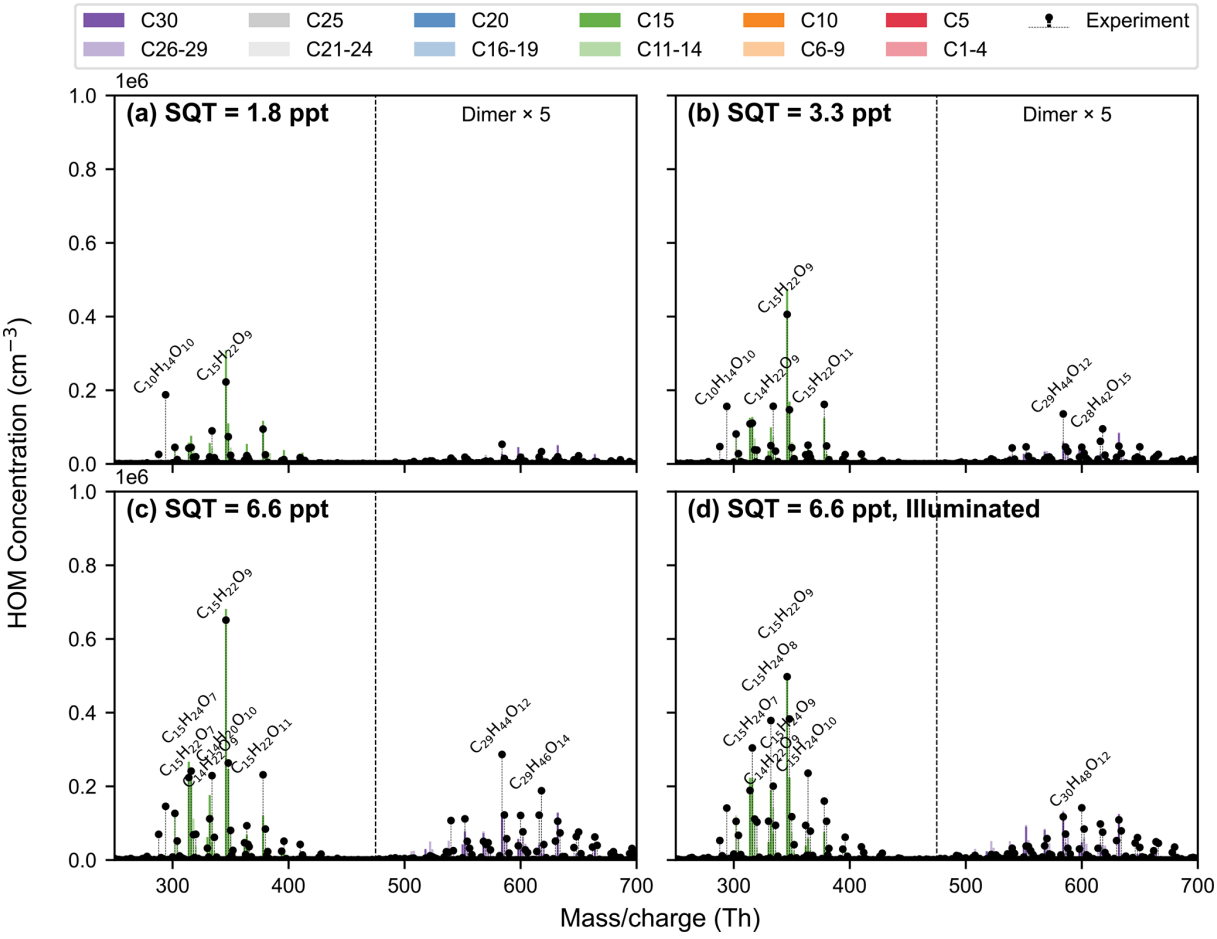

Figure 5. Comparisons between modeled and observed spectrum in β-caryophyllene oxidation experiment with **(a)** 1.8 ppt, **(b)** 3.3 ppt and **(c, d)** 6.6 ppt β-caryophyllene in **(a–c)** dark condition and **(d)** Hamamatsu UV lamps (UVH) on. Mass/charge ratio is plotted in units of thomsons (Th) and it should be noted that the nitrate reagent ions has been removed from mass.

4 Conclusion

In this study, we developed a novel and comprehensive mechanism, SIM-HOM (Sesquiterpene, Isoprene, and Monoterpene-derived HOM mechanism), for simulating the HOM formation from isoprene, monoterpenes, and sesquiterpenes. This mechanism incorporates intricate processes such as autoxidation and interactions among RO_2 radicals derived from various BVOC, providing a more nuanced understanding of the chemical transformations leading to HOM formation. The mechanism was rigorously optimized and validated using experimental data obtained from the CLOUD chamber, thereby demonstrating its robust capability to accurately reproduce the observed concentrations of HOMs under various conditions. From an atmospheric perspective, this model is particularly valuable for understanding NPF and SOA formation. Recent studies have highlighted the nucleating potential of isoprene-derived HOMs, a process that our mechanism captures effectively. In fact, our model is the only one capable of simulating isoprene HOMs, which represents a crucial advancement in understanding NPF. Another key innovation of our work is the refinement of the monoterpene oxidation mechanism, which was already recognized as crucial in previous models, but is now further optimized to improve its representation of HOM formation. Furthermore, the inclusion of sesquiterpene-derived HOMs, which are key contributors to NPF as shown in recent literature, makes this model the first to integrate these VOCs-derived HOM in a comprehensive framework. Importantly, the improved HOM parameterization introduced here bridges the gap between detailed gas-phase chemistry and aerosol-phase processes. It is increasingly recognized that not all HOM contribute equally to SOA formation: some exhibit low volatility and can irreversibly condense onto particles, while others are semi-volatile and may evaporate on short timescales. Our framework captures these differences by resolving HOM at a near-molecular level, thereby improving predictions of both short-lived SOA and more stable aerosol mass that influences air quality and climate-relevant properties, such as cloud formation. Overall, our model significantly enhances

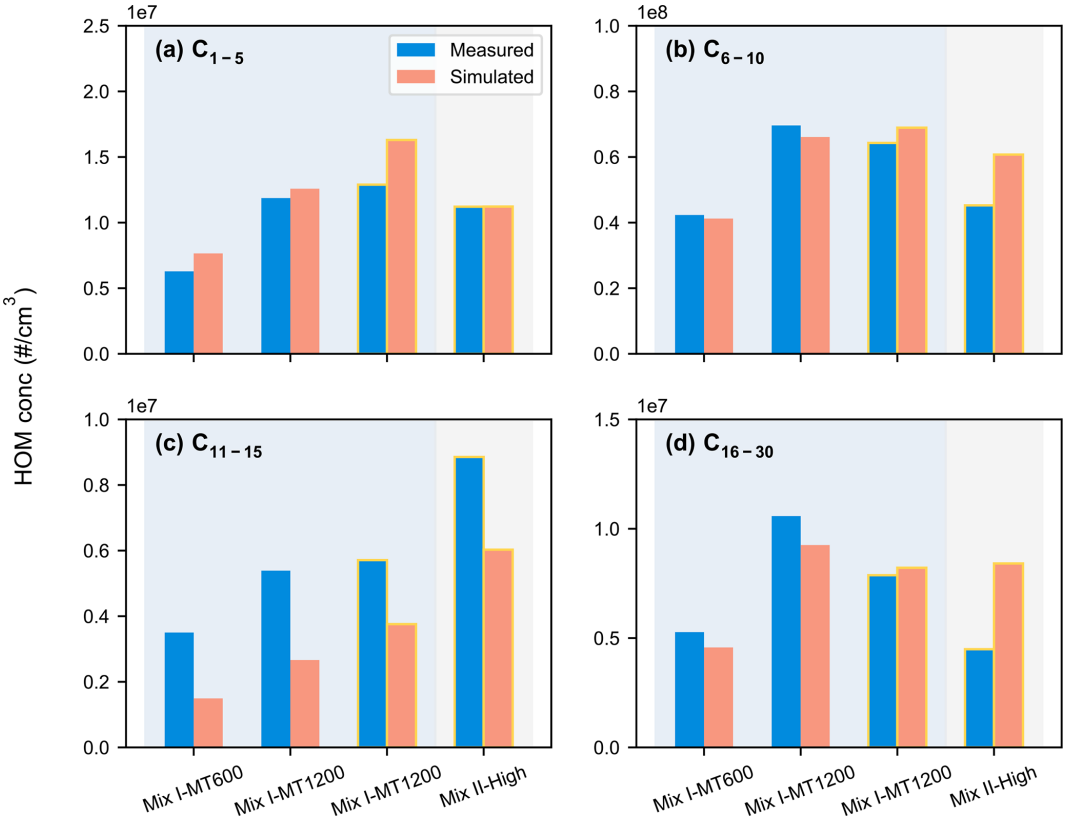

Figure 6. Experimental and simulated HOM concentration for different carbon numbers in four different mix systems (Mix I-MT600: 600 ppt α-pinene + 4 ppb isoprene; Mix I-MT1200: 1200 ppt α-pinene + 4 ppb isoprene; Mix I-MT1200: 1200 ppt α-pinene + 4 ppb isoprene, illuminated; Mix II-High: 1200 ppt α-pinene + 6 ppb isoprene + 16 ppt β-caryophyllene, illuminated, respectively). Blue bars indicate observed values and pink bars indicate simulated values, where no edge color indicates dark conditions and yellow edge color indicates light conditions. The light blue background indicates the mixed system I of isoprene and monoterpenes, and the grey background indicates the mixed system II of the three VOCs. The specific experimental conditions are shown in Table 1.

the ability of atmospheric simulations to link specific oxidation pathways to aerosol formation outcomes, thereby offering a more mechanistic foundation for understanding and predicting NPF and SOA formation across diverse environments.

However, several limitations need to be addressed. First, the model does not yet fully incorporate NO_x-related pathways. Given the significant role of NO_x in HOM formation, especially in polluted environments, refining these pathways is critical for improving predictions under high-NO_x conditions. In particular, the potential contribution of NO_3-initiated oxidation to HOM formation is not yet represented in the current version of the model. Recent studies suggest that the importance of NO_3 chemistry is strongly compound-dependent. For example, laboratory measurements indicate that HOM yields from isoprene + NO_3 reactions ($\sim 1.2\,\%$) (Zhao et al., 2021) are substantially higher than those from isoprene oxidation by O_3 or OH (Jokinen et al., 2015), implying that NO_3 chemistry may represent an important nighttime source of HOMs from isoprene. For larger BVOCs such as sesquiterpenes, their multiple double bonds and high reactivity may also favor rapid autoxidation following NO_3 addition, potentially leading to efficient HOM formation. In contrast, monoterpenes already exhibit substantial HOM production through O_3 and OH oxidation (Ehn et al., 2014; Kirkby et al., 2016), suggesting that NO_3 chemistry may play a less dominant role, although it could still contribute under certain nocturnal conditions. Due to the limited availability of systematic experimental data, particularly for isoprene and sesquiterpene NO_3 oxidation, these pathways are not yet explicitly included in the present mechanism and represent an important direction for future model development.

Additionally, the model does not yet incorporate photolysis reactions comprehensively, which can significantly alter the fate of HOMs and oxidation products under experimental conditions, such as utilizing UV lamps in the CLOUD chamber. Moreover, in the isoprene mechanism, multigenerational oxidation plays a crucial role, but its contribution to HOMs in laboratory experiments is likely lower than observed in the atmosphere. Another limitation lies in the branching ratios of key reactions, which govern the probability of different chemical pathways during autoxidation. Refining these

ratios will be essential for the model's predictive capability. Expanding the mechanism to include a wider range of VOCs and their oxidation products, and considering the influence of environmental factors like temperature and atmospheric composition, will further improve its applicability under diverse conditions.

Looking forward, an important challenge lies in simplifying the mechanism for integration into computationally efficient atmospheric models, such as global or regional climate models. While our mechanism provides valuable insights into the chemical processes of HOM formation, its complexity poses a challenge for large-scale simulations. Developing simplified parameterizations that retain the key atmospheric processes while reducing computational costs will be a key step in facilitating its integration into broader atmospheric models for climate and air quality forecasting. In conclusion, this model represents a significant advancement in understanding of HOM formation and its role in atmospheric processes. However, further improvements, especially in refining NO_x interactions, photolysis processes and constraining multigenerational oxidation in the isoprene system, are necessary to fully realize its potential. And efforts to simplify the mechanism for large-scale models, will be essential for broader implementation in atmospheric science and policy.

Code and data availability. The ADCHAM (version 1.0) code coupled with SIM-HOM (version 1.0) mechanism used in this study is publicly available at https://doi.org/10.5281/zenodo.19047874 (Yang et al., 2026). The repository also includes the model output generated in this study.

Supplement. The supplement related to this article is available online at https://doi.org/10.5194/gmd-19-5155-2026-supplement.

Author contributions. WN designed the study. LY performed model simulations and analyzed the data. WN, ME, CY, LD, YL, PR and AD are acknowledged for valuable discussions. LY and WN wrote the manuscript. ME and LD contributed to editing the manuscript.

Competing interests. The contact author has declared that none of the authors has any competing interests.

Disclaimer. Publisher's note: Copernicus Publications remains neutral with regard to jurisdictional claims made in the text, published maps, institutional affiliations, or any other geographical representation in this paper. The authors bear the ultimate responsibility for providing appropriate place names. Views expressed in the text are those of the authors and do not necessarily reflect the views of the publisher.

Acknowledgements. We thank CERN-CLOUD for providing experimental data, and the High-Performance Computing Center of Nanjing University for providing computing resources.

Financial support. This research has been supported by the National Key Research and Development Program of China (grant no. 2023YFC3706302), the National Natural Science Foundation of China (NSFC) (grant no. 42220104006), the Jiangsu Province Outstanding Youth Fund (grant no. BK20240067), the Natural Science Foundation of Jiangsu Province (grant no. BK20230773), the Jiangsu Provincial Collaborative Innovation Center of Climate Change, and the Fundamental Research Funds for the Central Universities.

Review statement. This paper was edited by Patrick Jöckel and reviewed by Paul Wennberg and Domenico Taraborrelli.

References

Bates, K. H. and Jacob, D. J.: A new model mechanism for atmospheric oxidation of isoprene: global effects on oxidants, nitrogen oxides, organic products, and secondary organic aerosol, Atmos. Chem. Phys., 19, 9613–9640, https://doi.org/10.5194/acp-19-9613-2019, 2019.

Berndt, T., Richters, S., Jokinen, T., Hyttinen, N., Kurten, T., Otkjaer, R. V., Kjaergaard, H. G., Stratmann, F., Herrmann, H., Sipila, M., Kulmala, M., and Ehn, M.: Hydroxyl radical-induced formation of highly oxidized organic compounds, Nat. Commun., 7, https://doi.org/10.1038/ncomms13677, 2016.

Berndt, T., Mender, B., Scholz, W., Fischer, L., Herrmann, H., Kulmala, M., and Hansel, A.: Accretion Product Formation from Ozonolysis and OH Radical Reaction of α-Pinene: Mechanistic Insight and the Influence of Isoprene and Ethylene, Environ. Sci. Technol., 52, 11069–11077, https://doi.org/10.1021/acs.est.8b02210, 2018.

Berndt, T., Hoffmann, E. H., Tilgner, A., and Herrmann, H.: Highly oxidized products from the atmospheric reaction of hydroxyl radicals with isoprene, Nat. Commun., 16, 12, https://doi.org/10.1038/s41467-025-57336-1, 2025.

Crounse, J. D., Nielsen, L. B., Jorgensen, S., Kjaergaard, H. G., and Wennberg, P. O.: Autoxidation of Organic Compounds in the Atmosphere, J. Phys. Chem. Lett., 4, 3513–3520, https://doi.org/10.1021/jz4019207, 2013.

Curtius, J., Heinritzi, M., Beck, L. J., Pöhlker, M. L., Tripathi, N., Krumm, B. E., Holzbeck, P., Nussbaumer, C. M., Pardo, L. H., Klimach, T., Barmpounis, K., Andersen, S. T., Bardakov, R., Bohn, B., Cecchini, M. A., Chaboureau, J. P., Dauhut, T., Dienhart, D., Dörich, R., Edtbauer, A., Giez, A., Hartmann, A., Holanda, B. A., Joppe, P., Kaiser, K., Keber, T., Klebach, H., Krüger, O. O., Kürten, A., Mallaun, C., Marno, D., Martinez, M., Monteiro, C., Nelson, C., Ort, L., Raj, S. S., Richter, S., Ringsdorf, A., Rocha, F., Simon, M., Sreekumar, S., Tsokankunku, A., Unfer, G. R., Valenti, I. D., Wang, N. J., Zahn, A., Zauner-Wieczorek, M., Albrecht, R. I., Andreae, M. O., Artaxo, P., Crowley, J. N., Fischer, H., Harder, H., Herdies, D. L., Machado, L. A. T., Pöhlker, C., Pöschl, U., Possner, A., Pozzer, A., Schnei-

der, J., Williams, J., and Lelieveld, J.: Isoprene nitrates drive new particle formation in Amazon's upper troposphere, Nature, 636, 23, https://doi.org/10.1038/s41586-024-08192-4, 2024.

Dada, L., Stolzenburg, D., Simon, M., Fischer, L., Heinritzi, M., Wang, M. Y., Xiao, M., Vogel, A. L., Ahonen, L., Amorim, A., Baalbaki, R., Baccarini, A., Baltensperger, U., Bianchi, F., Daellenbach, K. R., DeVivo, J., Dias, A., Dommen, J., Duplissy, J., Finkenzeller, H., Hansel, A., He, X. C., Hofbauer, V., Hoyle, C. R., Kangasluoma, J., Kim, C., Kürten, A., Kvashnin, A., Mauldin, R., Makhmutov, V., Marten, R., Mentler, B., Nie, W., Petäjä, T., Quéléver, L. L. J., Saathoff, H., Tauber, C., Tome, A., Molteni, U., Volkamer, R., Wagner, R., Wagner, A. C., Wimmer, D., Winkler, P. M., Yan, C., Zha, Q. Z., Rissanen, M., Gordon, H., Curtius, J., Worsnop, D. R., Lehtipalo, K., Donahue, N. M., Kirkby, J., El Haddad, I., and Kulmala, M.: Role of sesquiterpenes in biogenic new particle formation, Sci. Adv., 9, https://doi.org/10.1126/sciadv.adi5297, 2023.

D'Arnbro, E. L., Moller, K. H., Lopez-Hilfiker, F. D., Schobesberger, S., Liu, J. M., Shilling, J. E., Lee, B., Kjaergaard, H. G., and Thornton, J. A.: Isomerization of Second-Generation Isoprene Peroxy Radicals: Epoxide Formation and Implications for Secondary Organic Aerosol Yields, Environ. Sci. Technol., 51, 4978–4987, https://doi.org/10.1021/acs.est.7b00460, 2017.

Ehn, M., Thornton, J. A., Kleist, E., Sipila, M., Junninen, H., Pullinen, I., Springer, M., Rubach, F., Tillmann, R., Lee, B., Lopez-Hilfiker, F., Andres, S., Acir, I. H., Rissanen, M., Jokinen, T., Schobesberger, S., Kangasluoma, J., Kontkanen, J., Nieminen, T., Kurten, T., Nielsen, L. B., Jorgensen, S., Kjaergaard, H. G., Canagaratna, M., Dal Maso, M., Berndt, T., Petaja, T., Wahner, A., Kerminen, V. M., Kulmala, M., Worsnop, D. R., Wildt, J., and Mentel, T. F.: A large source of low-volatility secondary organic aerosol, Nature, 506, 476–479, https://doi.org/10.1038/nature13032, 2014.

Heinritzi, M., Dada, L., Simon, M., Stolzenburg, D., Wagner, A. C., Fischer, L., Ahonen, L. R., Amanatidis, S., Baalbaki, R., Baccarini, A., Bauer, P. S., Baumgartner, B., Bianchi, F., Brilke, S., Chen, D. X., Chiu, R., Dias, A., Dommen, J., Duplissy, J., Finkenzeller, H., Frege, C., Fuchs, C., Garmash, O., Gordon, H., Granzin, M., El Haddad, I., He, X. C., Helm, J., Hofbauer, V., Hoyle, C. R., Kangasluoma, J., Keber, T., Kim, C., Kürten, A., Lamkaddam, H., Laurila, T. M., Lampilahti, J., Lee, C. P., Lehtipalo, K., Leiminger, M., Mai, H. J., Makhmutov, V., Manninen, H. E., Marten, R., Mathot, S., Mauldin, R. L., Mentler, B., Molteni, U., Müller, T., Nie, W., Nieminen, T., Onnela, A., Partoll, E., Passananti, M., Petäjä, T., Pfeifer, J., Pospisilova, V., Quéléver, L. L. J., Rissanen, M. P., Rose, C., Schobesberger, S., Scholz, W., Scholze, K., Sipilä, M., Steiner, G., Stozhkov, Y., Tauber, C., Tham, Y. J., Vazquez-Pufleau, M., Virtanen, A., Vogel, A. L., Volkamer, R., Wagner, R., Wang, M. Y., Weitz, L., Wimmer, D., Xiao, M., Yan, C., Ye, P. L., Zha, Q. Z., Zhou, X. Q., Amorim, A., Baltensperger, U., Hansel, A., Kulmala, M., Tomé, A., Winkler, P. M., Worsnop, D. R., Donahue, N. M., Kirkby, J., and Curtius, J.: Molecular understanding of the suppression of new-particle formation by isoprene, Atmos. Chem. Phys., 20, 11809–11821, https://doi.org/10.5194/acp-20-11809-2020, 2020.

Iyer, S., Rissanen, M. P., Valiev, R., Barua, S., Krechmer, J. E., Thornton, J., Ehn, M., and Kurtén, T.: Molecular mechanism for rapid autoxidation in α-pinene ozonolysis, Nat. Commun., 12, 6, https://doi.org/10.1038/s41467-021-21172-w, 2021.

Jenkin, M. E., Young, J. C., and Rickard, A. R.: The MCM v3.3.1 degradation scheme for isoprene, Atmos. Chem. Phys., 15, 11433–11459, https://doi.org/10.5194/acp-15-11433-2015, 2015.

Jenkin, M. E., Valorso, R., Aumont, B., and Rickard, A. R.: Estimation of rate coefficients and branching ratios for reactions of organic peroxy radicals for use in automated mechanism construction, Atmos. Chem. Phys., 19, 7691–7717, https://doi.org/10.5194/acp-19-7691-2019, 2019.

Jokinen, T., Berndt, T., Makkonen, R., Kerminen, V. M., Junninen, H., Paasonen, P., Stratmann, F., Herrmann, H., Guenther, A. B., Worsnop, D. R., Kulmala, M., Ehn, M., and Sipilä, M.: Production of extremely low volatile organic compounds from biogenic emissions: Measured yields and atmospheric implications, P. Natl. Acad. Sci. USA, 112, 7123–7128, https://doi.org/10.1073/pnas.1423977112, 2015.

Jokinen, T., Kausiala, O., Garmash, O., Peräkylä, O., Junninen, H., Schobesberger, S., Yan, C., Sipilä, M., and Rissanen, M. P.: Production of highly oxidized organic compounds from ozonolysis of β-caryophyllene: laboratory and field measurements, Boreal Environ. Res., 21, 262–273, 2016.

Jorgensen, S., Knap, H. C., Otkjaer, R. V., Jensen, A. M., Kjeldsen, M. L. H., Wennberg, P. O., and Kjaergaard, H. G.: Rapid Hydrogen Shift Scrambling in Hydroperoxy-Substituted Organic Peroxy Radicals, J. Phys. Chem. A, 120, 266–275, https://doi.org/10.1021/acs.jpca.5b06768, 2016.

Kenseth, C. M., Hafeman, N. J., Rezgui, S. P., Chen, J., Huang, Y. L., Dalleska, N. F., Kjaergaard, H. G., Stoltz, B. M., Seinfeld, J. H., and Wennberg, P. O.: Particle-phase accretion forms dimer esters in pinene secondary organic aerosol, Science, 382, 787–792, https://doi.org/10.1126/science.adi0857, 2023.

Kirkby, J., Duplissy, J., Sengupta, K., Frege, C., Gordon, H., Williamson, C., Heinritzi, M., Simon, M., Yan, C., Almeida, J., Trostl, J., Nieminen, T., Ortega, I. K., Wagner, R., Adamov, A., Amorim, A., Bernhammer, A. K., Bianchi, F., Breitenlechner, M., Brilke, S., Chen, X. M., Craven, J., Dias, A., Ehrhart, S., Flagan, R. C., Franchin, A., Fuchs, C., Guida, R., Hakala, J., Hoyle, C. R., Jokinen, T., Junninen, H., Kangasluoma, J., Kim, J., Krapf, M., Kurten, A., Laaksonen, A., Lehtipalo, K., Makhmutov, V., Mathot, S., Molteni, U., Onnela, A., Perakyla, O., Piel, F., Petaja, T., Praplan, A. P., Pringle, K., Rap, A., Richards, N. A. D., Riipinen, I., Rissanen, M. P., Rondo, L., Sarnela, N., Schobesberger, S., Scott, C. E., Seinfeld, J. H., Sipila, M., Steiner, G., Stozhkov, Y., Stratmann, F., Tome, A., Virtanen, A., Vogel, A. L., Wagner, A. C., Wagner, P. E., Weingartner, E., Wimmer, D., Winkler, P. M., Ye, P. L., Zhang, X., Hansel, A., Dommen, J., Donahue, N. M., Worsnop, D. R., Baltensperger, U., Kulmala, M., Carslaw, K. S., and Curtius, J.: Ion-induced nucleation of pure biogenic particles, Nature, 533, 521–526, https://doi.org/10.1038/nature17953, 2016.

Knap, H. C. and Jorgensen, S.: Rapid Hydrogen Shift Reactions in Acyl Peroxy Radicals, J. Phys. Chem. A, 121, 1470–1479, https://doi.org/10.1021/acs.jpca.6b12787, 2017.

Krechmer, J. E., Coggon, M. M., Massoli, P., Nguyen, T. B., Crounse, J. D., Hu, W. W., Day, D. A., Tyndall, G. S., Henze, D. K., Rivera-Rios, J. C., Nowak, J. B., Kimmel, J. R., Mauldin, R. L., Stark, H., Jayne, J. T., Sipilä, M., Junninen, H., St

Clair, J. M., Zhang, X., Feiner, P. A., Zhang, L., Miller, D. O., Brune, W. H., Keutsch, F. N., Wennberg, P. O., Seinfeld, J. H., Worsnop, D. R., Jimenez, J. L., and Canagaratna, M. R.: Formation of Low Volatility Organic Compounds and Secondary Organic Aerosol from Isoprene Hydroxyhydroperoxide Low-NO Oxidation, Environ. Sci. Technol., 49, 10330–10339, https://doi.org/10.1021/acs.est.5b02031, 2015.

Lehtipalo, K., Yan, C., Dada, L., Bianchi, F., Xiao, M., Wagner, R., Stolzenburg, D., Ahonen, L. R., Amorim, A., Baccarini, A., Bauer, P. S., Baumgartner, B., Bergen, A., Bernhammer, A. K., Breitenlechner, M., Brilke, S., Buchholz, A., Mazon, S. B., Chen, D. X., Chen, X. M., Dias, A., Dommen, J., Draper, D. C., Duplissy, J., Ehn, M., Finkenzeller, H., Fischer, L., Frege, C., Fuchs, C., Garmash, O., Gordon, H., Hakala, J., He, X. C., Heikkinen, L., Heinritzi, M., Helm, J. C., Hofbauer, V., Hoyle, C. R., Jokinen, T., Kangasluoma, J., Kerminen, V. M., Kim, C., Kirkby, J., Kontkanen, J., Kürten, A., Lawler, M. J., Mai, H. J., Mathot, S., Mauldin, R. L., Molteni, U., Nichman, L., Nie, W., Nieminen, T., Ojdanic, A., Onnela, A., Passananti, M., Petäjä, T., Piel, F., Pospisilova, V., Quéléver, L. L. J., Rissanen, M. P., Rose, C., Sarnela, N., Schallhart, S., Schuchmann, S., Sengupta, K., Simon, M., Sipilä, M., Tauber, C., Tomé, A., Tröstl, J., Väisänen, O., Vogel, A. L., Volkamer, R., Wagner, A. C., Wang, M. Y., Weitz, L., Wimmer, D., Ye, P. L., Ylisirniö, A., Zha, Q. Z., Carslaw, K. S., Curtius, J., Donahue, N. M., Flagan, R. C., Hansel, A., Riipinen, I., Virtanen, A., Winkler, P. M., Baltensperger, U., Kulmala, M., and Worsnop, D. R.: Multicomponent new particle formation from sulfuric acid, ammonia, and biogenic vapors, Sci. Adv., 4, https://doi.org/10.1126/sciadv.aau5363, 2018.

Liu, Y., Nie, W., Qi, X., Li, Y., Xu, T., Liu, C., Ge, D., Chen, L., Niu, G., Wang, J., Yang, L., Wang, L., Zhu, C., Wang, J., Zhang, Y., Liu, T., Zha, Q., Yan, C., Ye, C., Zhang, G., Hu, R., Huang, R.-J., Chi, X., Zhu, T., and Ding, A.: The Pivotal Role of Heavy Terpenes and Anthropogenic Interactions in New Particle Formation on the Southeastern Qinghai-Tibet Plateau, Environ. Sci. Technol., 58, 19748–19761, https://doi.org/10.1021/acs.est.4c04112, 2024.

Liu, Y. L., Nie, W., Li, Y. Y., Ge, D. F., Liu, C., Xu, Z. N., Chen, L. D., Wang, T. Y., Wang, L., Sun, P., Qi, X. M., Wang, J. P., Xu, Z., Yuan, J., Yan, C., Zhang, Y. J., Huang, D. D., Wang, Z., Donahue, N. M., Worsnop, D., Chi, X. G., Ehn, M., and Ding, A. J.: Formation of condensable organic vapors from anthropogenic and biogenic volatile organic compounds (VOCs) is strongly perturbed by NO_x in eastern China, Atmos. Chem. Phys., 21, 14789–14814, https://doi.org/10.5194/acp-21-14789-2021, 2021.

Liu, Y. L., Liu, C., Nie, W., Li, Y. Y., Ge, D. F., Chen, L. D., Zhu, C. J., Wang, L., Zhang, Y. X., Liu, T. Y., Qi, X. M., Wang, J. P., Huang, D. D., Wang, Z., Yan, C., Chi, X. G., and Ding, A. J.: Exploring condensable organic vapors and their co-occurrence with $PM_{2.5}$ and O_3 in winter in Eastern China, Environm. Sci.-Atmos., 3, 282–297, https://doi.org/10.1039/d2ea00143h, 2023.

McFiggans, G., Mentel, T. F., Wildt, J., Pullinen, I., Kang, S., Kleist, E., Schmitt, S., Springer, M., Tillmann, R., Wu, C., Zhao, D. F., Hallquist, M., Faxon, C., Le Breton, M., Hallquist, A. M., Simpson, D., Bergstrom, R., Jenkin, M. E., Ehn, M., Thornton, J. A., Alfarra, M. R., Bannan, T. J., Percival, C. J., Priestley, M., Topping, D., and Kiendler-Scharr, A.: Secondary organic aerosol reduced by mixture of atmospheric vapours, Nature, 565, 587–593, https://doi.org/10.1038/s41586-018-0871-y, 2019.

Meder, M., Graeffe, F., Luo, Y., Luo, J., Iyer, S., Valiev, R., Cai, R., Rissanen, M., Kurtén, T., Varelas, J. G., Geiger, F. M., Thomson, R. J., and Ehn, M.: Selective Deuteration Reveals the Importance of Multiple Branching Pathways in α-Pinene Autoxidation, J. Am. Chem. Soc., 147, 14131–14138, https://doi.org/10.1021/jacs.4c14462, 2025.

Moller, K. H., Otkjær, R. V., Hyttinen, N., Kurtén, T., and Kjaergaard, H. G.: Cost-Effective Implementation of Multiconformer Transition State Theory for Peroxy Radical Hydrogen Shift Reactions, J. Phys. Chem. A, 120, 10072–10087, https://doi.org/10.1021/acs.jpca.6b09370, 2016.

Moller, K. H., Bates, K. H., and Kjaergaard, H. G.: The Importance of Peroxy Radical Hydrogen-Shift Reactions in Atmospheric Isoprene Oxidation, J. Phys. Chem. A, 123, 920–932, https://doi.org/10.1021/acs.jpca.8b10432, 2019.

Murphy, S. E., Crounse, J. D., Poulsen, A. S., Lipson, J. E., Kjaergaard, H. G., and Wennberg, P. O.: Accretion product formation in the self- and cross-reactions of small β-hydroxy peroxy radicals, Environ. Sci.-Atmos., 5, 1312–1325, https://doi.org/10.1039/d5ea00106d, 2025.

Ng, N. L., Kwan, A. J., Surratt, J. D., Chan, A. W. H., Chhabra, P. S., Sorooshian, A., Pye, H. O. T., Crounse, J. D., Wennberg, P. O., Flagan, R. C., and Seinfeld, J. H.: Secondary organic aerosol (SOA) formation from reaction of isoprene with nitrate radicals (NO_3), Atmos. Chem. Phys., 8, 4117–4140, https://doi.org/10.5194/acp-8-4117-2008, 2008.

Nguyen, T. B., Coggon, M. M., Bates, K. H., Zhang, X., Schwantes, R. H., Schilling, K. A., Loza, C. L., Flagan, R. C., Wennberg, P. O., and Seinfeld, J. H.: Organic aerosol formation from the reactive uptake of isoprene epoxydiols (IEPOX) onto non-acidified inorganic seeds, Atmos. Chem. Phys., 14, 3497–3510, https://doi.org/10.5194/acp-14-3497-2014, 2014.

Nguyen, T. B., Bates, K. H., Crounse, J. D., Schwantes, R. H., Zhang, X., Kjaergaard, H. G., Surratt, J. D., Lin, P., Laskin, A., Seinfeld, J. H., and Wennberg, P. O.: Mechanism of the hydroxyl radical oxidation of methacryloyl peroxynitrate (MPAN) and its pathway toward secondary organic aerosol formation in the atmosphere, Phys. Chem. Chem. Phys., 17, 17914–17926, https://doi.org/10.1039/c5cp02001h, 2015.

Nie, W., Yan, C., Huang, D. D., Wang, Z., Liu, Y., Qiao, X., Guo, Y., Tian, L., Zheng, P., Xu, Z., Li, Y., Xu, Z., Qi, X., Sun, P., Wang, J., Zheng, F., Li, X., Yin, R., Dallenbach, K. R., Bianchi, F., Petäjä, T., Zhang, Y., Wang, M., Schervish, M., Wang, S., Qiao, L., Wang, Q., Zhou, M., Wang, H., Yu, C., Yao, D., Guo, H., Ye, P., Lee, S., Li, Y. J., Liu, Y., Chi, X., Kerminen, V.-M., Ehn, M., Donahue, N. M., Wang, T., Huang, C., Kulmala, M., Worsnop, D., Jiang, J., and Ding, A.: Secondary organic aerosol formed by condensing anthropogenic vapours over China's megacities, Nat. Geosci., 15, 255–261, https://doi.org/10.1038/s41561-022-00922-5, 2022.

Nie, W., Yan, C., Yang, L., Roldin, P., Liu, Y., Vogel, A. L., Molteni, U., Stolzenburg, D., Finkenzeller, H., Amorim, A., Bianchi, F., Curtius, J., Dada, L., Draper, D. C., Duplissy, J., Hansel, A., He, X.-C., Hofbauer, V., Jokinen, T., Kim, C., Lehtipalo, K., Nichman, L., Mauldin, R. L., Makhmutov, V., Mentler, B., Mizelli-Ojdanic, A., Petäjä, T., Quéléver, L. L. J., Schallhart, S., Simon, M., Tauber, C., Tomé, A., Volkamer, R., Wagner, A. C., Wagner,

R., Wang, M., Ye, P., Li, H., Huang, W., Qi, X., Lou, S., Liu, T., Chi, X., Dommen, J., Baltensperger, U., El Haddad, I., Kirkby, J., Worsnop, D., Kulmala, M., Donahue, N. M., Ehn, M., and Ding, A.: NO at low concentration can enhance the formation of highly oxygenated biogenic molecules in the atmosphere, Nat. Commun., 14, 3347, https://doi.org/10.1038/s41467-023-39066-4, 2023.

Otkjaer, R. V., Jakobsen, H. H., Tram, C. M., and Kjaergaard, H. G.: Calculated Hydrogen Shift Rate Constants in Substituted Alkyl Peroxy Radicals, J. Phys. Chem. A, 122, 8665–8673, https://doi.org/10.1021/acs.jpca.8b06223, 2018.

Paulot, F., Crounse, J. D., Kjaergaard, H. G., Kürten, A., St Clair, J. M., Seinfeld, J. H., and Wennberg, P. O.: Unexpected Epoxide Formation in the Gas-Phase Photooxidation of Isoprene, Science, 325, 730–733, https://doi.org/10.1126/science.1172910, 2009.

Peräkylä, O., Berndt, T., Franzon, L., Hasan, G., Meder, M., Valiev, R. R., Daub, C. D., Varelas, J. G., Geiger, F. M., Thomson, R. J., Rissanen, M., Kurtén, T., and Ehn, M.: Large Gas-Phase Source of Esters and Other Accretion Products in the Atmosphere, J. Am. Chem. Soc., 145, 7780–7790, https://doi.org/10.1021/jacs.2c10398, 2023.

Praske, E., Otkjaer, R. V., Crounse, J. D., Hethcox, J. C., Stoltz, B. M., Kjaergaard, H. G., and Wennberg, P. O.: Atmospheric autoxidation is increasingly important in urban and suburban North America, P. Natl. Acad. Sci. USA, 115, 64–69, https://doi.org/10.1073/pnas.1715540115, 2018.

Riccobono, F., Schobesberger, S., Scott, C. E., Dommen, J., Ortega, I. K., Rondo, L., Almeida, J., Amorim, A., Bianchi, F., Breitenlechner, M., David, A., Downard, A., Dunne, E. M., Duplissy, J., Ehrhart, S., Flagan, R. C., Franchin, A., Hansel, A., Junninen, H., Kajos, M., Keskinen, H., Kupc, A., Kurten, A., Kvashin, A. N., Laaksonen, A., Lehtipalo, K., Makhmutov, V., Mathot, S., Nieminen, T., Onnela, A., Petaja, T., Praplan, A. P., Santos, F. D., Schallhart, S., Seinfeld, J. H., Sipila, M., Spracklen, D. V., Stozhkov, Y., Stratmann, F., Tome, A., Tsagkogeorgas, G., Vaattovaara, P., Viisanen, Y., Vrtala, A., Wagner, P. E., Weingartner, E., Wex, H., Wimmer, D., Carslaw, K. S., Curtius, J., Donahue, N. M., Kirkby, J., Kulmala, M., Worsnop, D. R., and Baltensperger, U.: Oxidation Products of Biogenic Emissions Contribute to Nucleation of Atmospheric Particles, Science, 344, 717–721, https://doi.org/10.1126/science.1243527, 2014.

Richters, S., Herrmann, H., and Berndt, T.: Highly Oxidized RO_2 Radicals and Consecutive Products from the Ozonolysis of Three Sesquiterpenes, Environ. Sci. Technol., 50, 2354–2362, https://doi.org/10.1021/acs.est.5b05321, 2016a.

Richters, S., Herrmann, H., and Berndt, T.: Different pathways of the formation of highly oxidized multifunctional organic compounds (HOMs) from the gas-phase ozonolysis of β-caryophyllene, Atmos. Chem. Phys., 16, 9831–9845, https://doi.org/10.5194/acp-16-9831-2016, 2016b.

Riva, M., Rantala, P., Krechmer, J. E., Peräkylä, O., Zhang, Y. J., Heikkinen, L., Garmash, O., Yan, C., Kulmala, M., Worsnop, D., and Ehn, M.: Evaluating the performance of five different chemical ionization techniques for detecting gaseous oxygenated organic species, Atmos. Meas. Tech., 12, 2403–2421, https://doi.org/10.5194/amt-12-2403-2019, 2019.

Roldin, P., Eriksson, A. C., Nordin, E. Z., Hermansson, E., Mogensen, D., Rusanen, A., Boy, M., Swietlicki, E., Svenningsson, B., Zelenyuk, A., and Pagels, J.: Modelling non-equilibrium secondary organic aerosol formation and evaporation with the aerosol dynamics, gas- and particle-phase chemistry kinetic multilayer model ADCHAM, Atmos. Chem. Phys., 14, 7953–7993, https://doi.org/10.5194/acp-14-7953-2014, 2014.

Roldin, P., Ehn, M., Kurtén, T., Olenius, T., Rissanen, M. P., Sarnela, N., Elm, J., Rantala, P., Hao, L., Hyttinen, N., Heikkinen, L., Worsnop, D. R., Pichelstorfer, L., Xavier, C., Clusius, P., Öström, E., Petäjä, T., Kulmala, M., Vehkamäki, H., Virtanen, A., Riipinen, I., and Boy, M.: The role of highly oxygenated organic molecules in the Boreal aerosol-cloud-climate system, Nat. Commun., 10, 4370, https://doi.org/10.1038/s41467-019-12338-8, 2019.

Schervish, M. and Donahue, N. M.: Peroxy radical chemistry and the volatility basis set, Atmos. Chem. Phys., 20, 1183–1199, https://doi.org/10.5194/acp-20-1183-2020, 2020.

Schervish, M., Heinritzi, M., Stolzenburg, D., Dada, L., Wang, M. Y., Ye, Q., Hofbauer, V., Devivo, J., Bianchi, F., Brilke, S., Duplissy, J., El Haddad, I., Finkenzeller, H., He, X. C., Kvashnin, A., Kim, C., Kirkby, J., Kulmala, M., Lehtipalo, K., Lopez, B., Makhmutov, V., Mentler, B., Molteni, U., Nie, W., Petäjä, T., Quéléver, L., Volkamer, R., Wagner, A. C., Winkler, P., Yan, C., and Donahue, N. M.: Interactions of peroxy radicals from monoterpene and isoprene oxidation simulated in the radical volatility basis set, Environ. Sci.-Atmos., 4, 740–753, https://doi.org/10.1039/d4ea00056k, 2024.

Shen, H. R., Vereecken, L., Kang, S. A., Pullinen, I., Fuchs, H., Zhao, D. F., and Mentel, T. F.: Unexpected significance of a minor reaction pathway in daytime formation of biogenic highly oxygenated organic compounds, Sci. Adv., 8, https://doi.org/10.1126/sciadv.abp8702, 2022.

Shen, J. L., Russell, D. M., Devivo, J., Kunkler, F., Baalbaki, R., Mentler, B., Scholz, W., Yu, W. J., Caudillo-Plath, L., Sommer, E., Ahongshangbam, E., Alfaouri, D., Almeida, J., Amorim, A., Beck, L. J., Beckmann, H., Berntheusel, M., Bhattacharyya, N., Canagaratna, M. R., Chassaing, A., Cruz-Simbron, R., Dada, L., Duplissy, J., Gordon, H., Granzin, M., Schute, L. G., Heinritzi, M., Iyer, S., Klebach, H., Krueger, T., Kuerten, A., Lampimaeki, M., Liu, L., Lopez, B., Martinez, M., Morawiec, A., Onnela, A., Peltola, M., Rato, P., Reza, M., Richter, S., Roerup, B., Sebastian, M. K., Simon, M., Surdu, M., Tamme, K., Thakur, R. C., Tome, A., Tong, Y. D., Top, J., Umo, N. S., Unfer, G., Vettikkat, L., Weissbacher, J., Xenofontos, C., Yang, B. X., Zauner-Wieczorek, M., Zhang, J. Y., Zheng, Z. S., Baltensperger, U., Christoudias, T., Flagan, R. C., El Haddad, I., Junninen, H., Moehler, O., Riipinen, I., Rohner, U., Schobesberger, S., Volkamer, R., Winkler, P. M., Hansel, A., Lehtipalo, K., Donahue, N. M., Lelieveld, J., Harder, H., Kulmala, M., Worsnop, D. R., Kirkby, J., Curtius, J., and He, X. C.: New particle formation from isoprene under upper-tropospheric conditions, Nature, 636, https://doi.org/10.1038/s41586-024-08196-0, 2024.

Simon, M., Dada, L., Heinritzi, M., Scholz, W., Stolzenburg, D., Fischer, L., Wagner, A. C., Kurten, A., Rorup, B., He, X. C., Almeida, J., Baalbaki, R., Baccarini, A., Bauer, P. S., Beck, L., Bergen, A., Bianchi, F., Brakling, S., Brilke, S., Caudillo, L., Chen, D. X., Chu, B. W., Dias, A., Draper, D. C., Duplissy, J., El-Haddad, I., Finkenzeller, H., Frege, C., Gonzalez-Carracedo, L., Gordon, H., Granzin, M., Hakala, J., Hofbauer, V., Hoyle, C. R., Kim, C., Kong, W. M., Lamkaddam, H., Lee, C. P., Lehtipalo, K., Leiminger, M., Mai, H. J., Manninen, H. E., Marie, G.,

Marten, R., Mentler, B., Molteni, U., Nichman, L., Nie, W., Ojdanic, A., Onnela, A., Partoll, E., Petaja, T., Pfeifer, J., Philippov, M., Quelever, L. L. J., Ranjithkumar, A., Rissanen, M. P., Schallhart, S., Schobesberger, S., Schuchmann, S., Shen, J. L., Sipila, M., Steiner, G., Stozhkov, Y., Tauber, C., Tham, Y. J., Tome, A. R., Vazquez-Pufleau, M., Vogel, A. L., Wagner, R., Wang, M. Y., Wang, D. S., Wang, Y. H., Weber, S. K., Wu, Y. S., Xiao, M., Yan, C., Ye, P. L., Ye, Q., Zauner-Wieczorek, M., Zhou, X. Q., Baltensperger, U., Dommen, J., Flagan, R. C., Hansel, A., Kulmala, M., Volkamer, R., Winkler, P. M., Worsnop, D. R., Donahue, N. M., Kirkby, J., and Curtius, J.: Molecular understanding of new-particle formation from alpha-pinene between −50 and +25 °C, Atmos. Chem. Phys., 20, 9183–9207, https://doi.org/10.5194/acp-20-9183-2020, 2020.

Sindelarova, K., Granier, C., Bouarar, I., Guenther, A., Tilmes, S., Stavrakou, T., Müller, J. F., Kuhn, U., Stefani, P., and Knorr, W.: Global data set of biogenic VOC emissions calculated by the MEGAN model over the last 30 years, Atmos. Chem. Phys., 14, 9317–9341, https://doi.org/10.5194/acp-14-9317-2014, 2014.

Stolzenburg, D., Fischer, L., Vogel, A. L., Heinritzi, M., Schervish, M., Simon, M., Wagner, A. C., Dada, L., Ahonen, L. R., Amorim, A., Baccarini, A., Bauer, P. S., Baumgartner, B., Bergen, A., Bianchi, F., Breitenlechner, M., Brilke, S., Mazon, S. B., Chen, D. X., Dias, A., Draper, D. C., Duplissy, J., Haddad, I., Finkenzeller, H., Frege, C., Fuchs, C., Garmash, O., Gordon, H., He, X., Helm, J., Hofbauer, V., Hoyle, C. R., Kim, C., Kirkby, J., Kontkanen, J., Kuerten, A., Lampilahti, J., Lawler, M., Lehtipalo, K., Leiminger, M., Mai, H., Mathot, S., Mentler, B., Molteni, U., Nie, W., Nieminen, T., Nowak, J. B., Ojdanic, A., Onnela, A., Passananti, M., Petaja, T., Quelever, L. L. J., Rissanen, M. P., Sarnela, N., Schallhart, S., Tauber, C., Tome, A., Wagner, R., Wang, M., Weitz, L., Wimmer, D., Xiao, M., Yan, C., Ye, P., Zha, Q., Baltensperger, U., Curtius, J., Dommen, J., Flagan, R. C., Kulmala, M., Smith, J. N., Worsnop, D. R., Hansel, A., Donahue, N. M., and Winkler, P. M.: Rapid growth of organic aerosol nanoparticles over a wide tropospheric temperature range, P. Natl. Acad. Sci. USA, 115, 9122–9127, https://doi.org/10.1073/pnas.1807604115, 2018.

Sun, H., Liu, Y., Nie, W., Li, Y., Ge, D., Xu, T., Yin, J., Liu, C., Fu, Z., Qi, X., Liu, T., Zha, Q., Yan, C., Wang, Z., Chi, X., and Ding, A.: Unexpected Gas-Phase Formation of Glycolic Acid Sulfate in the Atmosphere, Environ. Sci. Technol., 59, 16556–16566, https://doi.org/10.1021/acs.est.5c07888, 2025.

Trostl, J., Chuang, W. K., Gordon, H., Heinritzi, M., Yan, C., Molteni, U., Ahlm, L., Frege, C., Bianchi, F., Wagner, R., Simon, M., Lehtipalo, K., Williamson, C., Craven, J. S., Duplissy, J., Adamov, A., Almeida, J., Bernhammer, A. K., Breitenlechner, M., Brilke, S., Dias, A., Ehrhart, S., Flagan, R. C., Franchin, A., Fuchs, C., Guida, R., Gysel, M., Hansel, A., Hoyle, C. R., Jokinen, T., Junninen, H., Kangasluoma, J., Keskinen, H., Kim, J., Krapf, M., Kurten, A., Laaksonen, A., Lawler, M., Leiminger, M., Mathot, S., Mohler, O., Nieminen, T., Onnela, A., Petaja, T., Piel, F. M., Miettinen, P., Rissanen, M. P., Rondo, L., Sarnela, N., Schobesberger, S., Sengupta, K., Sipila, M., Smith, J. N., Steiner, G., Tome, A., Virtanen, A., Wagner, A. C., Weingartner, E., Wimmer, D., Winkler, P. M., Ye, P. L., Carslaw, K. S., Curtius, J., Dommen, J., Kirkby, J., Kulmala, M., Riipinen, I., Worsnop, D. R., Donahue, N. M., and Baltensperger, U.: The role of low-volatility organic compounds in initial particle growth in the atmosphere, Nature, 533, 527–531, https://doi.org/10.1038/nature18271, 2016.

Wang, S. N., Riva, M., Yan, C., Ehn, M., and Wang, L. M.: Primary Formation of Highly Oxidized Multifunctional Products in the OH-Initiated Oxidation of Isoprene: A Combined Theoretical and Experimental Study, Environ. Sci. Technol., 52, 12255–12264, https://doi.org/10.1021/acs.est.8b02783, 2018.

Weber, J., Archer-Nicholls, S., Griffiths, P., Berndt, T., Jenkin, M., Gordon, H., Knote, C., and Archibald, A. T.: CRI-HOM: A novel chemical mechanism for simulating highly oxygenated organic molecules (HOMs) in global chemistry-aerosol-climate models, Atmos. Chem. Phys., 20, 10889–10910, https://doi.org/10.5194/acp-20-10889-2020, 2020.

Wennberg, P. O., Bates, K. H., Crounse, J. D., Dodson, L. G., McVay, R. C., Mertens, L. A., Nguyen, T. B., Praske, E., Schwantes, R. H., Smarte, M. D., St Clair, J. M., Teng, A. P., Zhang, X., and Seinfeld, J. H.: Gas-Phase Reactions of Isoprene and Its Major Oxidation Products, Chem. Rev., 118, 3337–3390, https://doi.org/10.1021/acs.chemrev.7b00439, 2018.

Xu, Z. N., Nie, W., Liu, Y. L., Sun, P., Huang, D. D., Yan, C., Krechmer, J., Ye, P. L., Xu, Z., Qi, X. M., Zhu, C. J., Li, Y. Y., Wang, T. Y., Wang, L., Huang, X., Tang, R. Z., Guo, S., Xiu, G. L., Fu, Q. Y., Worsnop, D., Chi, X. G., and Ding, A. J.: Multifunctional Products of Isoprene Oxidation in Polluted Atmosphere and Their Contribution to SOA, Geophys. Res. Lett., 48, https://doi.org/10.1029/2020gl089276, 2021.

Yang, H., Raucci, U., Iyer, S., Hasan, G., Almeida, T. G., Barua, S., Savolainen, A., Kangasluoma, J., Rissanen, M., Vehkamäki, H., and Kurtén, T.: Molecular dynamics-guided reaction discovery reveals endoperoxide-to-alkoxy radical isomerization as key branching point in α-pinene ozonolysis, Nat. Commun., 16, 12, https://doi.org/10.1038/s41467-025-55985-w, 2025a.

Yang, L., Nie, W., Yan, C., Ehn, M., Liu, Y., Roldin, P., Qi, X., Kerminen, V.-M., Donahue, N. M., Worsnop, D., Kulmala, M., and Ding, A.: A mechanistic understanding of the varying yields of highly oxygenated organic molecules, Nat. Commun., 17, 302, https://doi.org/10.1038/s41467-025-67007-w, 2025b.

Yang, L., Roldin, P., and Nie, W.: SIM-HOM model (version 1.0), Zenodo [code], https://doi.org/10.5281/zenodo.19047874, 2026.

Zha, Q. Z., Aliaga, D., Krejci, R., Sinclair, V. A., Wu, C., Ciarelli, G., Scholz, W., Heikkinen, L., Partoll, E., Gramlich, Y., Huang, W., Leiminger, M., Enroth, J., Peräkylä, O., Cai, R. L., Chen, X. M., Koenig, A. M., Velarde, F., Moreno, I., Petäjä, T., Artaxo, P., Laj, P., Hansel, A., Carbone, S., Kulmala, M., Andrade, M., Worsnop, D., Mohr, C., and Bianchi, F.: Oxidized organic molecules in the tropical free troposphere over Amazonia, Natl. Sci. Rev., 11, 11, https://doi.org/10.1093/nsr/nwad138, 2024.

Zhao, D. F., Pullinen, I., Fuchs, H., Schrade, S., Wu, R. R., Acir, I. H., Tillmann, R., Rohrer, F., Wildt, J., Guo, Y. D., Kiendler-Scharr, A., Wahner, A., Kang, S., Vereecken, L., and Mentel, T. F.: Highly oxygenated organic molecule (HOM) formation in the isoprene oxidation by NO_3 radical, Atmos. Chem. Phys., 21, 9681–9704, https://doi.org/10.5194/acp-21-9681-2021, 2021.